A Thesis for the Degree of Ph.D. in Science

Electron paramagnetic resonance of photoexcited triplet states of oxygen-vacancy centers in silicon

March 2012

Graduate School of Science and Technology
Keio University

Akhtar Mohammad Waseem

Abstract

Spin-based quantum computation is one of the most ambitious applications of spintronic where the electron and/or nuclear spins are employed as quantum bits (qubits). In the scheme of semiconductor silicon-based quantum computing, electron spins and nuclear spins of phosphorus donors and nuclear spins of ^{29}Si have attracted much attention as candidates for qubits. However, neither physical processes to transfer quantum information into and out of a particular spin qubit nor methods to exchange information between spin qubits have been established.

The present thesis shows that the presence of photoexcited triplet electron spins of oxygen-vacancy centers (SL1 centers) in silicon establishes a novel way to induce spin flip-flops of the triplet spins with phosphorus electron spins even in the absence of electromagnetic excitation field. Moreover, SL1 center is shown to be an excellent center to transfer quantum information into and out of ^{29}Si nuclear spin qubits.

The thesis is composed of six chapters. Chapter 1 is an introduction which includes the motivation and the detail description of the spin systems utilized in this work. Chapter 2 provides the basic principles of magnetic resonance techniques employed in this work.

Chapter 3 shows the spin dependent recombination processes via phosphorus donor states and SL1 triplet states in silicon detected by the change in the photoconductivity of samples. This corresponds to electrically detected magnetic resonance (EDMR) of electron and nuclear spin states of phosphorus and SL1, i. e., electrical readout of spin qubit states in silicon. Furthermore electrical detection of cross relaxation (EDCR), flip-flops between phosphorus bound electron spins and SL1 triplet spins, is shown. When the Zeeman splittings of the dipolar coupled phosphorus electron and photoexcited triplet electron spins are made equal by appropriate tuning of the external magnetic field, they undergo flip-flop transitions which change the overall recombination of the photoexcited carriers and thus changing the photoconductivity of the sample.

Chapter 4 investigates the lifetime of the photoexcited triplet SL1 centers and their interaction with the nearest-neighbor ^{29}Si nuclear spins using pulsed electron paramagnetic spin resonane (pEPR). While the population rates of the three triplet levels are almost equal, the decay rate from each triplet level to the ground singlet state is found to be different leading to $\approx$100% spin polarization in about 1.5 ms after creation of the photoexcited states by the laser pulse. The electron spin echo envelop modulation

reveals the hyperfine coupling of the triplet electron spins with the nearest-neighbor nuclear spins of ^{29}Si (I=1/2).

Chapter 5 describes a proof-of-concept operation of ^{29}Si nuclear spin quantum memory in silicon. The coupling between the highly polarized triplet electron spins and ^{29}Si nuclear spins facilitate the transfer and storage of the coherent state of the triplet electron spins in the nuclear spin degrees of freedom using a series of resonant microwave and radio frequency pulses in the pulse electron nuclear double resonance (pENDOR). We found nuclear storage time of nearly 5 ms which is close to the previously reported T_{2n} of 5.6 ms for ^{29}S.

Finally summary and outlook are provided in Chapter 6.

Acknowledgements

It has been nearly three years in Itoh group and would like to acknowledge most of the people who directly or indirectly contributed towards the completion of this thesis.

I sincerely thank my supervisor Professor Kohei M. Itoh for giving me an oppertunity to pursue this work under his guidence and for the fruitful discussions that we had on the topics related to this work. His useful comments and criticism has certainly helped me in becoming a better researcher and motivated me to keep the pace of my research. Well, all I can say is that he was the person without whose support, it would have been difficult to achieve this feat. The second person who comes to mind when i talk about guidence in my PhD is certainly Professor Leonid Vlasenko. My interaction with him really helped me in understanding my research and get some exciting results. I would also like to thank Dr. John Morton of Oxford University who really helped me in the latter part of my PhD work. I am really greatful to him for giving me the chance to work in his group and perform some exciting experiments. I also learned a lot about writing articles and about some experimental techniques.

I am really thankful to the Professor Eiji Ohta, Professor Junko Hayase, Professor Yoichi Kamihara and Professor Leonid Vlasenko for reveiwing this research work and for their kind comments for improving the thesis.

I would like to thank Aizawa-san for her unconditional support and always helping me in preparing documents those were in japanese. I also thank Prof. Uematsu for discussions and for his help while performing some ion implantation simulation.

My special thanks to Dr. Hiroki Morishita for teaching me the experimental techniques used for electrical detection of magnetic resonance. I am highly oblige to Dr. Takeharu Sekiguchi for taking out time for lengthy discussions that helped me a lot in understanding the various pulse sequences utilized in this work. I would also thank Dr. Vasilea Filidau for helping me in my work at Oxford University and for her warm hospitality during my visit to UK.

Although few of the group members were directly involved in my project, their research activities, spirits, opinions, and other right things affected me in several ways, and all the other past and present group members are worthy of acknowledgements. A sincerely acknowledge the support from the laboratory members namely, Dr. Satoru Miyamoto, Dr. Hiroki Morishita, Dr. Mohammad Rizwanur Rahman, Toy-

ofumi Ishikawa, Yoko Kawamura, Itahashi Tatsumasa, Shinichi Tojo, Hiroyuki Tezuka, Masashi Hirose, Nao Harada, Miki Nganawa, Kei Yoshizawa, Shinchan Hong Agung, Luis Jou Garcia, Rii Hirano, Katsuhiko Naito, Go tsuchiya, Yuri Sakuma, Kei Koga and Tomoya Arai, all of whom really made my research journey a memorable one. One person who has always been very helpful, supportive and really entertainer is Matsuaka Takashi, a final year master student at our laboratory. I wish him and all others a very best for their future endeavors.

I am really grateful to Dr. Mohammad Rizwanur Rahman and Dr. Vijay Raj Singh for making the stay in Japan a memorable one. Finally, I would like to thank my friends and my family who supported me all along these years. My family has been a really backbone for me throughout my life and their love and support has encouraged me to overcome the difficulties throughout this research life. A special thanks to my fiance whose unconditional support has motivated me and helped me in focusing on my work.

On the financial aspect, this work was supported in part by Grant-in-Aid for Scientific Research and Project for Developing Innovation Systems by MEXT, FIRST, Keio G-COE and JST-EPSRC/SIC (EP/H025952/1). I am thankful to them for funding this research.

Contents

1 Introduction **1**

1.1 Background and motivation 1

1.1.1 Spin based quantum computer 1

1.1.2 Phosphorus (^{31}P) in silicon 3

1.1.3 ^{29}Si nuclear spin in silicon 5

1.2 Triplet state: Two interacting electrons 6

1.2.1 Photoexcited Triplets 9

1.2.2 Unique properties of photoexcited triplets 10

1.3 Photoextied triplets in silicon: SL1 centers 12

1.4 Organization of thesis 15

Bibliography **16**

2 Magnetic Resonance **20**

2.1 Introduction 21

2.1.1 Electron magnetic moment and its interaction with magnetic field 21

2.2 Pulsed Electron Paramagnetic Resonance 25

2.2.1 Hahn echo method 25

2.2.2 Spin-Spin Interaction 26

2.3 Electrically detected magnetic resonance 29

Bibliography **32**

3 Spin dependent recombination processes in phosphorus doped γ-irradiated silicon **33**

3.1 Electrically detected magnetic resonance 34

3.1.1 Introduction 35

3.1.2 Experimental 36

3.1.3 Results and discussions 36

3.1.4 Conclusion 40

3.2 Electrically detected cross relaxation 41

3.2.1 Introduction 42

3.2.2 Experimental 44

3.2.3 EDMR and EDCR spectra 45
3.2.4 Angular dependence of EDCR line positions 48
3.2.5 Model for the observed photoconductivity change under cross relaxation 50
3.2.6 Conclusion 54

Bibliography **55**

4 pEPR study of SL1 center **58**
4.1 Lifetime of photoexcited triplets:SL1 centers 59
4.2 Electron spin echo envelop modulation 64
4.3 Conclusion 69

Bibliography **70**

5 Coherent storage of photoexcited triplet states using ^{29}Si nuclear spins in silicon **71**
5.1 Introduction 72
5.2 Experimental 72
5.3 Coherent state transfer between photoexcited triplets electron spin and ^{29}Si nuclear spin in silicon 74
5.4 Conclusion 78

Bibliography **79**

6 Summary **81**
6.1 Summary 81

Chapter 1

Introduction

1.1 Background and motivation

1.1.1 Spin based quantum computer

The massive increase in computational power of contemporary digital computers (classical computers) is a direct result of the successful drive to build devices on smaller and smaller scales. However, there is a physical limit to this process of miniaturization and soon a stage will be reached when we will have systems working on atomic scales governed fully by quantum phenomena. This leads to the idea of building a quantum computer based entirely on the quantum phenomena [1]. Computers whose operation is based on the fundamental principles of quantum mechanics promise to outperform even the fastest conceivable classical computers [2]. The two main elements for the realization of these quantum computers are 1) data representation by quantum bits (qubits) and 2) quantum gates to manipulate qubits to perform logical operation. A classical computer has a memory made up of bits, where each bit represents either a state $|\psi\rangle = |0\rangle$ or $|\psi\rangle = |1\rangle$ state . However, its counterpart QCs utilizes the quantum two level systems as quantum bits (qubits) where the qubits can be in any of the valid superposition states of $|0\rangle$ and $|1\rangle$, i.e. $|\psi\rangle = \alpha\,|0\rangle + \beta\,|1\rangle$. Such a vector can be visualized on the Bloch sphere shown in Figure 1.1 as $|\psi\rangle = \cos(\theta/2)\,|0\rangle + e^{i\phi/2}\sin(\theta/2)\,|1\rangle$.

The corruption of this quantum state can be due to: the corruption of θ which is also known as spin lattice relaxation time $T_1$and also due to the corruption of ϕ known as decoherence time T_2. In order to harness the enormous capability of a QCs we need to look for physical system where the qubits can be scaled, initialized and manipulated on a much faster time scale than its decoherence time. And finally, the read out of the final state of the qubits should be feasible.

So far there has been many quantum system proposed as a qubits. Prominent example includes atoms in cavities, trapped ions and liquid state nuclear magnetic resonance (NMR) where the first few quantum system which attracted researchers worldwide for the realization of QCs [3, 4, 5]. However, all the above mentioned system face the prob-

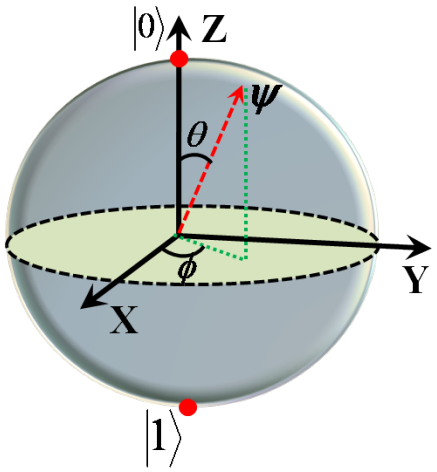

Figure 1.1: Bloch sphere - Bloch sphere representation of a vector.

lem of scalability. The requirement for the scalability motivated researchers to propose solid state quantum computer based on electron spin qubits ("up" spin and "down" spin: two level quantum system). In that regard, electron confined to GaAs quantum dots have been proposed [6]. But due to the interaction with the 100% nuclear matrix and the spin-orbit interactions in these systems, electron spin dephases on a much faster time scale.

Silicon based quantum computer has an advantage of the well developed semiconductor technology that would be needed for integration of devices. The added advantage of silicon lies in the isotopic engineering which allows having an isolated spin free bath for quantum system. There has been two very promising proposals in silicon: 1) Kanes quantum computer [7] and 2) All silicon quantum computer [8, 9].

1) Kanes quantum computer: It was Bruce Kane in 1998 who proposed an idea of utilizing an array of phosphorus atoms in silicon as qubits (shown in Figure 1.2(a)). Phosphorus is a hydrogenic donor in silicon having an electron spin S=1/2 and a nuclear spin I=1/2. In the proposed architecture for QC, individual donors could be addressed by tuning the hyperfine interaction between the electron and nuclear spin with application of electrostatic bias directly above the donor position (A-gate). This changes the energy levels of the donor spin states and thus making the donor resonant or non-resonant with the globally applied radio frequency field. Two qubit operations are performed by tuning the exchange interaction between the donors with J-gate placed between the A-gates.

2) All silicon quantum computer : Silicon has three stable isotopes namely, ^{28}Si,

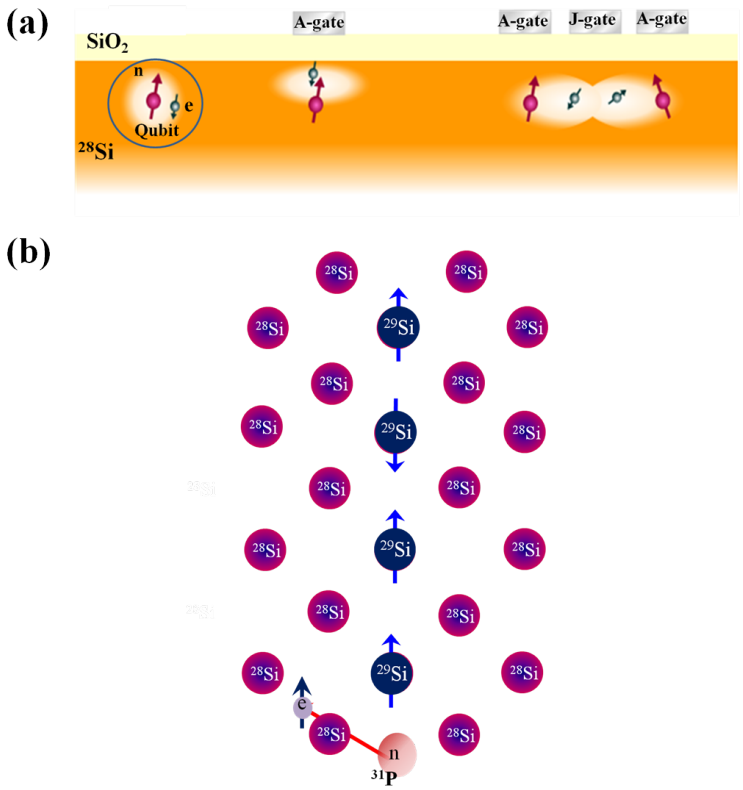

Figure 1.2: Quantum computer model - (a) Kanes quantum computer. (b) All silicon quantum computer.

^{29}Si and ^{30}Si, out of which only ^{29}Si has a nuclear spin I=1/2. The proposed all silicon quantum computer utilizes the linear chain of these nuclear spins as qubits embedded in the spin free matrix of ^{28}Si (Figure 1.2(b)). With application of large magnetic field gradient the nuclear spins in the linear chain can be addressed selectively by resonant radio frequency pulses. The readout can be done using magnetic resonance force microscopy where the nuclear spin state couples to the vibrational mode of the cantilever. The other method for readout could be the use of hyperfine coupling of the nuclear spins with the electron spins of donors.

1.1.2 Phosphorus (^{31}P) in silicon

Phosphorus (^{31}P) in silicon is one of the most studied group V donors in silicon [10, 7]. ^{31}P has an electron spin S=1/2 and a nuclear spin I=1/2. At helium temperature the electron is bound to the phosphorus atom and the Hamiltonian for such a system in the presence of external magnetic field can be written as:

$$\mathcal{H}_{\text{Si:P}} = g_e\mu_B BS_z - g_n\mu_n BI_z + a\mathbf{S}\cdot\mathbf{I}, \tag{1.1}$$

where $\mathbf{S}$ and $\mathbf{I}$ are electron and phosphorus nuclear spins, respectively. Here $g_e\mu_B/2\pi\hbar \approx$ 28 GHz/T and $g_n\mu_n/2\pi\hbar \approx 17.2$ MHz/T are given by electron and nuclear g-factors $g_e \approx 1.9985$ and $g_n \approx 2.2632$, respectively.The hyperfine constant is $a/2\pi\hbar \approx 117.5$ MHz.

The third term represents the hyperfine interaction between phosphorus electron and nuclear spins, respectively. In high field regime, the Zeeman terms are much greater than the hyperfine term and we have pure states represented as

$$|1\rangle = |\uparrow\uparrow\rangle, \tag{1.2}$$
$$|2\rangle = |\uparrow\downarrow\rangle, \tag{1.3}$$
$$|3\rangle = |\downarrow\uparrow\rangle, \tag{1.4}$$
$$|4\rangle = |\downarrow\downarrow\rangle, \tag{1.5}$$

Si:P quantum system can be thought of as a two qubit quantum computer: for example, the controlled NOT operation where the electron spin flips conditioned by the state of the hyperfine coupled nuclear spin can be realized by exciting the EPR transition $|\downarrow_e\uparrow_n\rangle : |\uparrow_e\uparrow_n\rangle$, the SWAP operation [11] can be realized by exciting the transition $|\downarrow_e\uparrow_n\rangle : |\uparrow_e\downarrow_n\rangle$. Other significant advantage is the isotopic engineering of silicon allows to have well isolated donors in silicon due to which long coherence time of nearly 60 msec for ^{31}P electron spins and 2 sec for nuclear spin (limited by the spin relaxation time of the bound electron) has been measured [12, 11]. Add to this the recent experimental demonstration of entanglement between the coupled electron-nuclear spin of phosphorus in silicon, one of the essential requirements for quantum information processor [13].

However, the successful implementation of phosphorus in silicon for quantum computing application will require readout of single spin states. However, current EPR spectrometer has a much lower sensitivity and would be difficult to monitor single spins. But highly sensitive electrical method, electrically detected magnetic resonance (EDMR), could be employed for the readout of small number of spins. In this thesis we will demonstrate that the γ-irradiation defects in silicon can be used to probe electron and nuclear spin of phosphorus in silicon by EDMR spectroscopy. We will further demonstrate the electrical detection of cross relaxation in silicon due to the flip-flop

transition between the dipolar coupled electron spin of phosphorus and photoexcited triplet SL1 center.

1.1.3 ^{29}Si nuclear spin in silicon

Crystalline silicon is the most widely used semiconductor for the integrated circuits and most of the modern technology depends on it. Naturally available silicon is composed of three stable isotopes : ^{28}Si 92.2 %, ^{29}Si 4.7 %, and ^{30}Si 3.1 %. Out of these isotopes, only ^{29}Si has a nuclear spin of I=1/2. These nuclear spin embedded in the spin free matrix of ^{28}Si has been proposed as a qubit. The isotopic engineering associated with silicon would allow having an extremely isolated ^{29}Si nuclear spin system. Such isolated spin system is bound to have very long coherence time. The coherence time of the nuclear spin in natural silicon measured using Hahn echo pulse sequence [14] was found to be nearly 5.6 ms limited mainly by the dipolar interaction between the nuclear spins in the lattice [15]. Using NMR decoupling pulse sequence it was shown that the coherence time can be enhanced to 25 sec [16]. Such long coherence time is one of the criteria for nuclear spin to be utilized as memory qubit. However, challenges ahead are the initialization and the read out of the nuclear spin states. Due to the small magnetic moment associated with nuclear spin, the thermal equilibrium polarization of the nuclear spin system at experimentally accessed condition is very small. Two efficient way of polarizing the nuclear spin system is dynamic nuclear polarization (DNP) and optical nuclear polarization (ONP). ONP of ^{29}Si nuclear spin in silicon was first demonstrated by Lampel way back in 1968 where simple illumination of n-type silicon with circularly polarized light at 77 K lead to the nuclear polarization enhancement of about 28000 resulting in nuclear polarization of 0.0007% [17]. Recently, ONP under illumination with linearly polarized light, the cross relaxation of the ^{29}Si nuclear spins with non-thermal electron spins lead to the nuclear polarization of nearly 0.25% by working at helium temperature and high magnetic field 7 T [18]. The other indirect way of nuclear polarization is DNP technique where we transfer the spin polarization within the electron spin of the paramagnetic centers in the lattice at magnetic field B and temperature T to the nuclear spin under saturation of the EPR lines. A detail investigation of EPR induced DNP of ^{29}Si nuclear spin has been reported by Hayashi et. al where it was found that the DNP degree depends upon the ^{29}Si concentration as well as on the spin lattice relaxation time of the electron spin [19]. Very recently a nuclear polarization of 10% was achieved in n-type ([P]$\approx 10^{17}$) natural silicon working at magnetic field of 2.4 T and temperature 1.1 K [20]. The use of pseudo pure state

can reduce the physical requirement for the nuclear spin polarization however its still desirable to have perfectly initialization of nuclear spin qubits $\approx$ 100% for quantum computing application. Moreover, the read out of the ^{29}Si nuclear spin state is still illusive.

In this thesis we will show a way to achieve 100% polarization of ^{29}Si nuclear spin. Furthermore, the interaction between the triplet electron spin and the nuclear spin allows us to manipulate and read out nuclear spin state via photoexcited triplets in silicon. We also show transfer and storage of quantum information in nuclear spin thus demonstrating a feasibility of realizing ^{29}Si nuclear spin memory in silicon.

1.2 Triplet state: Two interacting electrons

Let us consider a system containing two electrons. According to Pauli's exclusion principle the total wavefunction of the system must be antisymmetric with respect to the exchange of space and spin coordinates of the two particles. The total wave function can be written as a product of a space wave function and a spin wave function, i.e.,

$$\psi_{total} = \psi\beta \tag{1.6}$$

where ψ is the space wave function and β is the spin wave function. Antisymmetry of the total wave function can be obtained by multiplying a symmetric space wave function with an antisymmetric spin wave function or vice versa.

Now, if the two electron (1 and 2) are in the spin triplet S=1 state, i.e., the spins of the two electrons are parallel then the spin wave function is symmetric.

$$S = 1 \begin{cases} {\beta_1}^+{\beta_2}^+ \equiv |1,+1\rangle \\ \frac{1}{\sqrt{2}}[{\beta_1}^+{\beta_2}^- + {\beta_1}^-{\beta_2}^+] \equiv |1,0\rangle \\ {\beta_1}^-{\beta_2}^- \equiv |1,-1\rangle \end{cases}$$

where + and − represents the up and down spin state of the electrons. The states are also represented by the *ket* using the notation $|S, m_s\rangle$. The wave function in the position space must be antisymmetric.

On the other hand if the two electrons are antiparallel,i.e., the overall spin S=0, the spin wave function is antisymmetric.

$$S = 0 \begin{cases} \frac{1}{\sqrt{2}}[{\beta_1}^+{\beta_2}^- - {\beta_1}^-{\beta_2}^+] \equiv |0,0\rangle \end{cases}$$

Thus, the antisymmetric wave function give rise to a singlet state while three symmetric wave function give rise to a three triplet states. All these four states are degenerate as long as we neglect any interaction between the electrons. However, the singlet and triplet states split apart in energy by the electron-exchange interaction, represented by the spin Hamiltonian:

$$\mathcal{H}_{exch} = \sum_{ij} \boldsymbol{J}_{ij} S_{1i} \cdot S_{2j}, \tag{1.7}$$

where S_1 and S_2 are the electron spin-operators for electron 1 and 2, respectively. Indices i and j label spatial coordinates(i,j=x,y,z). The most dominant part of the exchange-energy operator is given as:

$$(\mathcal{H}_{exch})_{iso} = J_0 S_1 \cdot S_2,$$

where $J_0 = \mathrm{tr}(\boldsymbol{J})/3$ is the isotropic electron-exchange coupling constant, which to a first approximation is given by the exchange integral:

$$J_0 = -2 \left\langle \psi_1(r_1)\psi_2(r_2) \mid \frac{e^2}{4\pi\varepsilon_0 r} \mid \psi_1(r_2)\psi_2(r_1) \right\rangle, \tag{1.8}$$

where $\psi_1(r_1)$ and $\psi_2(r_2)$ are the position space wave function of the two electrons, ε_0 is the permitivity of the vacuum and r is the inter-electron separation. This exchange is just one manifestation of the Coulomb interaction between two electrons. The singlet and triplet states are separated by the energy $\mid J_0 \mid$. The sign of J_0 determines whether the singlet or the triplet energy state lies lower. Figure 1.3 shows the energy levels of the singlet and triplet states for $J_0 > 0$ as a function of magnetic field.

In addition to electron-exchange, which splits the states into a singlet and triplets, there exists another important interaction, the anisotropic magnetic dipole-dipole interaction. This interaction lifts the three-fold degeneracy of the triplet state in zero magnetic field. The electron spin-spin dipolar interaction is given by the Hamiltonian

$$\mathcal{H}_{ss} = \hbar^2 {\gamma_e}^2 \left[\frac{\boldsymbol{S}_1 \cdot \boldsymbol{S}_2}{r^3} - \frac{3(\boldsymbol{S}_1 \cdot \boldsymbol{r})(\ \boldsymbol{S}_2 \cdot \boldsymbol{r})}{r^5} \right], \tag{1.9}$$

Because the two electrons are coupled, it is more convenient to express $\mathcal{H}_{ss}$ in terms of the total spin operator $\mathbf{S}$, defined by $\mathbf{S} = \mathbf{S_1} + \mathbf{S_2}$. Substituting this, together with the angular momentum commutation relation and the identity r^2=x^2+y^2+z^2, Eqn. 1.9 can be written in the matrix form as:

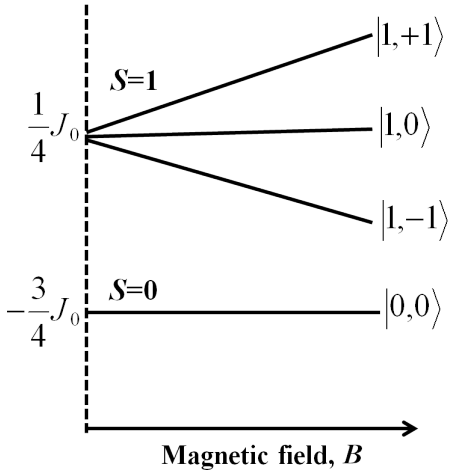

Figure 1.3: Exchange Interaction - The energy states of the two electron spin system exhibiting exchange interaction J_0 greater than zero.

$$\mathcal{H}_{ss} = \frac{\hbar^2 {\gamma_e}^2}{2} \begin{bmatrix} S_x & S_y & S_z \end{bmatrix} \cdot \begin{bmatrix} \left\langle \frac{r^2-3x^2}{r^5} \right\rangle & \left\langle \frac{-3xy}{r^5} \right\rangle & \left\langle \frac{-3xz}{r^5} \right\rangle \\ \left\langle \frac{-3xy}{r^5} \right\rangle & \left\langle \frac{r^2-3y^2}{r^5} \right\rangle & \left\langle \frac{-3yz}{r^5} \right\rangle \\ \left\langle \frac{-3xz}{r^5} \right\rangle & \left\langle \frac{-3yz}{r^5} \right\rangle & \left\langle \frac{r^2-3z^2}{r^5} \right\rangle \end{bmatrix} \cdot \begin{bmatrix} S_x \\ S_y \\ S_z \end{bmatrix} \quad (1.10)$$

The above euqation can be represented as $\mathcal{H}_{ss} = \mathbf{S} \cdot \mathbf{D} \cdot \mathbf{S}$, where $\mathbf{D}$ represent the spin-spin dipolar interaction tensor and the trace of the matrix is zero, i.e., $tr(\mathbf{D}) = 0$.The angular brakets indicate that the elements of the parameter matrix $\mathbf{D}$ are averages over the electronic spatial wave function. $\mathbf{D}$ can be diagonalized. Eqn.1.10 can be re-written in the principle-axis system (X, Y, and Z) of $\mathbf{D}$ as:

$$\mathcal{H}_{ss} = D_X {S_X}^2 + D_Y {S_Y}^2 + D_Z {S_Z}^2, \quad (1.11)$$

Here we introduce two parameters D and E, where D=$3/2 D_Z$ and $E = 1/2(D_X\text{-}D_Y)$ and are known as zero field parameter. Thus,

$$\mathcal{H}_{ss} = D({S_Z}^2 - \frac{1}{2}S^2) + E({S_X}^2 + {S_Y}^2), \quad (1.12)$$

In the present of the external magnetic field the total Hamiltonian of the triplet is given as

$$\mathcal{H}_e = \gamma_e \hbar \boldsymbol{B} \cdot \boldsymbol{S} + D({S_Z}^2 - \frac{1}{2}S^2) + E({S_X}^2 + {S_Y}^2), \quad (1.13)$$

The eigenfunction of $\mathcal{H}_e$ is linear combination of the kets $|+1\rangle$,$|0\rangle$ and $|-1\rangle$. In the limit $B \to 0$ with **B** parallel to the principle axis Z, the zero field triplet eigenfunctions are:

$$\begin{aligned} |T_X\rangle &= \frac{1}{\sqrt{2}}(|-1\rangle - |+1\rangle), \\ |T_Y\rangle &= \frac{i}{\sqrt{2}}(|-1\rangle + |+1\rangle), \\ |T_Z\rangle &= |0\rangle\,, \end{aligned} \tag{1.14}$$

1.2.1 Photoexcited Triplets

Upon photoexcitation, the ground singlet state of the two interacting electrons can be easily excited to triplet state. The formation of triplets are due to intersystem crossing from the the excited singlet via spin-orbit coupling [21]. The photoexcited triplets are metastable state and would eventually decay to the singlet ground state of the system. However, the transition from the triplet to the ground singlet state is generally forbidden, which gives triplet state a certain lifetime before it decays. The probability k_m of transition "to and from" triplet $T_m(m_s = 0, \pm 1)$ is proportional to the square of the matrix element of the spin-orbit coupling operator $\mathcal{H}_{SO}$:

$$k_m \propto |\langle S\,|\mathcal{H}_{SO}|\,T_M\rangle|^2 \tag{1.15}$$

The spin orbit coupling is defined as

$$\mathcal{H}_{SO} = \lambda \boldsymbol{L}\cdot\boldsymbol{S} \tag{1.16}$$

where λ is the scalar constant. The direct calculation of the matrix element of this operator yields

$$\begin{aligned} \langle S_0\,|\mathcal{H}_{SO}|\,T_\pm\rangle &= \frac{\lambda\hbar}{\sqrt{2}}(\langle\psi_1\,|l_x|\,\psi_2\rangle + i\,\langle\psi_1\,|l_y|\,\psi_2\rangle), \\ \langle S_0\,|\mathcal{H}_{SO}|\,T_0\rangle &= -\frac{\lambda\hbar}{\sqrt{2}}\langle\psi_1\,|l_z|\,\psi_2\rangle, \end{aligned} \tag{1.17}$$

Equation 1.17 shows that the triplet sublevels have different transition probability. These spin selective transition would lead to the non-equilibrium population of magnetic sublevels of triplet states (see Figure 1.4). Such non-equilibrium electron polarization [22, 23] can be utilized to polarize nuclear spin system in the host, which otherwise has very weak polarization at experimentally accessible conditions .

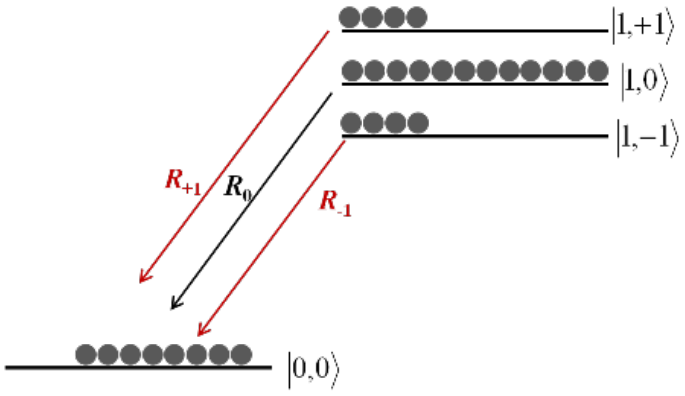

Figure 1.4: Non-equilibrium polarization - Schematic showing the singlet and triplet energy levels in the presence of external magnetic field B parallel to Z-axis of the triplet paramagnetic center. Selective transition to the ground singlet state under spin-orbit coupling builds high electron spin polarization in the triplet spin system.

1.2.2 Unique properties of photoexcited triplets

The ground singlet state of two interacting electron spins can be photoexcited to the triplet state. The spin orbit coupling which induces intersystem crossing to preferentially populate particular triplet sublevel and/or different decay rate from the triplet sublevels to the ground singlet state builds high spin polarization within the triplet spin system [21, 22]. Moreover, the dipolar interaction between the electron spins in the triplet state give rise to strong zero-field splitting [25]. These unique properties exhibited by photoexcited triplets has been exploited for the development of new magnetic resonance techniques such as single molecule optically detected magnetic resonance [24] and zero field EPR [25]. Using continuous microwave illumination (under processes termed dynamic nuclear polarization) [26, 27], or using microwave pulses [28], highly polarized electron spin triplets can be used to polarize surrounding nuclear spins which otherwise owing to its small magnetic moment has very weak thermal polarization at experimentally accessible conditions. Triplet states can also be used to mediate entanglement between mutually-coupled nuclear spins [29], on timescales much faster than their intrinsic dipolar coupling [30], thus suggesting the usefulness of photoexcited triplets as an optically driven mediator spins to couple nuclear spins in the lattice for quantum computing application [31]. These properties associated with the photoexcited triplets motivated us to study them in silicon and explore the microscopic processes exhibited by these spin system using magnetic resonance technique.

In this chapter, we will discuss about the triplet spin system in general and then

give a brief introduction of the photoexcited triplet spin system in silicon relevant for this thesis.

1.3 Photoextied triplets in silicon: SL1 centers

Oxygen and carbon are two major electrically inactive impurities always present in the silicon crystal, where oxygen takes the interstitial position while carbon is present at the sustitutional position. A lot of electrically active defect involving these two impurities are known to be formed as a result of radiation damage [32, 33]. The vacancy-oxygen complex (or A-centre) is the most prominent defect in either irradiated or implanted Si material. Its microscopic structure has been established by EPR and its vibrational properties by IR-absorption spectroscopy [33, 34, 35, 36]. This consists of an oxygen atom bridging a pair of Si neighbours of the vacancy. This defect is only stable when neutral and singly negatively charged. A deep single acceptor level or electron-trap at 0.17 eV below the conduction band minimum (E_c - 0.17 eV) [34] is associated with the negetive charged state of oxygen-vacancy complex (A-center).

In this thesis we focus on the photoexcited triplet states of these oxygen-vacancy complex in silicon, also known as SL1 center. It was first observed by Brower in 1972 using EPR spectroscopy [37] . SL1 center has orthorhombic symmetry of g and D-tensors with the principal values g_1 = 2.0057, g_2 = 2.0075, g_3 = 2.0102 and D_1 = -657 MHz, D_2 = 350 MHz, D_3 = 307 MHz corresponding to the principal axes 1, 2 and 3 parallel to [110], [100], and [1$\bar{1}$0] crystal axes, respectively (see Figure 1.5).

In silicon lattice the SL1 centers have six equivalent orientations along six different $\langle 110 \rangle$ crystal axes shown in Figure 1.5 by dashed lines. When the magnetic field B_0 is rotated in (1$\bar{1}$0) plane varying the angle θ from 0° to 90° with respect to [110], the angle between B_0 and principal axis 1 for one of six groups of SL1 centers oriented along line [ad] is also varied from 0° (B||[110]) to 90° (B||[001]). For second group with the principal axis 3 parallel to line [eh], the angle between B_0 and these centers is always equal to 90°. Remaining four groups of SL1 centers make the intermediate angle with respect to direction of magnetic field. Two groups of these centers oriented along [bh] and [be] are magneto-equivalent (with the same angle between B_0 and [bh] or [be] directions) as well as the groups oriented along [ag] and [af]. In the conclusion, it needs to consider only four orientations of SL1 centers in silicon lattice along [ad], [eh], [bh], and [ag] directions.

EPR and spin dependent recombination studies on these centers has revealed that the formation of triplets takes place due to simultaneous capture of photoexcited electron and hole by the ground singlet state of O-V complex [38]. Figure 1.6 shows the schematic for the formation of triplets , SL1 center under bandgap illumination. The

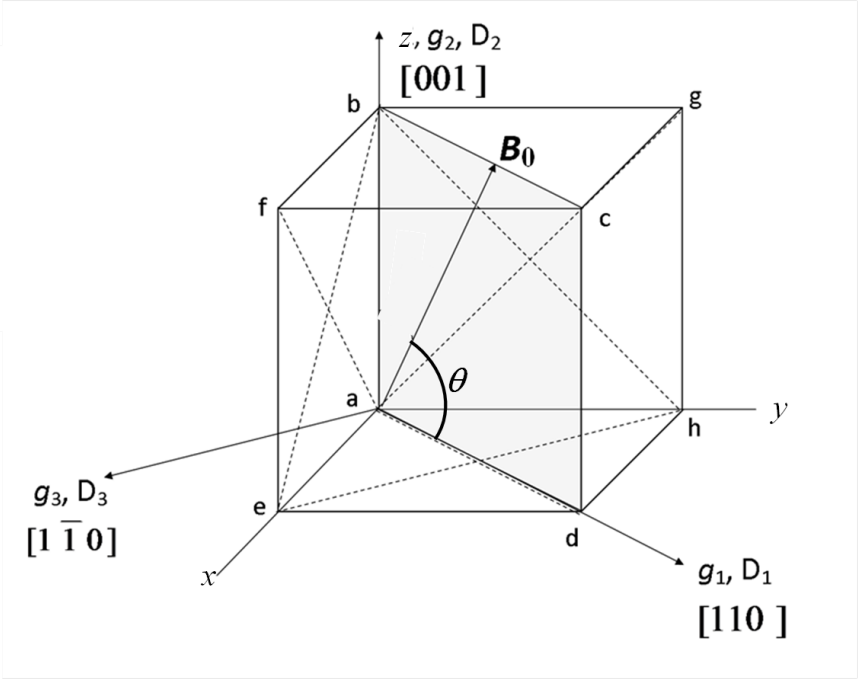

Figure 1.5: Orientation of SL1 centers - Pictorial representation of the SL1 structure in silicon lattice. It also shows the principle axis system of the defect.

non-equilibrium spin polarization in these triplets was confirmed by the observation of absorption and emission EPR signal simultaneously [37].

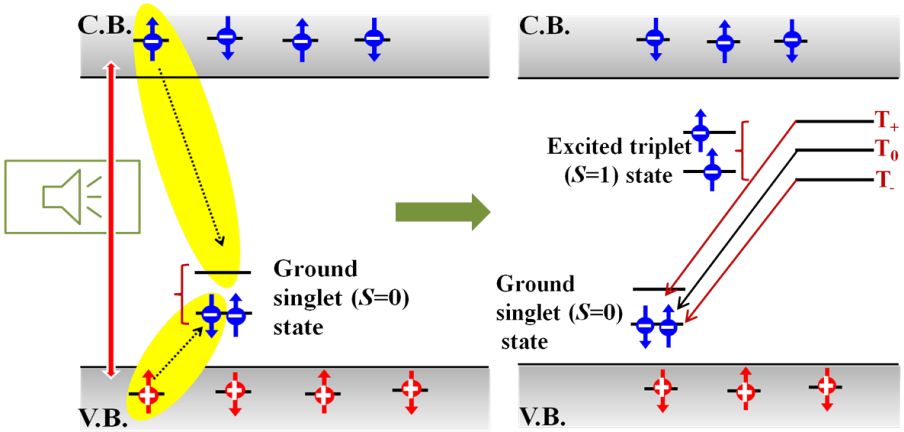

Figure 1.6: Formation of SL1 center under photoexcitation - The shcematic showing the photoexcitation of singlet ground state of oxygen-vacancy complex to the triplet state on simultaneous capturing of photoexcited carriers. The triplet population are equally filled initially but the selective transition to the ground singlet state builds the spin polarization in the sublevels.

The non-equilibrium polarization of SL1 center has been previously used to hyperpolarize the ^{29}Si nuclear spins using optical and dynamic nuclear polarization technique [39, 40]. Such hyperpolarized nuclear spin system in silicon would be a step towards the realization of recent proposal of ^{29}Si nuclear spin based quantum computer [8, 9]. The experimental demonstration of long coherence time for ^{29}Si nuclear spin in silicon makes it really an exciting system for quantum computing [16]. However, till date the quantum computing scheme using host stable isotope in solid has been demonstrated only with ^{13}C nuclear spins in diamond via coherent coupling to the spin-triplet nitrogen-vacancy centers [41, 42, 43].

Here we explore the electronic properties of SL1 center using electrical and conventional magnetic resonance technique and demonstrate that the interaction of these triplet centers with other electron and nuclear spin in the lattice leads to some exciting and interesting physics. We have demonstrated a well designed set of experiments to provide new information on spin-spin interactions between defect centers that can lead to the change in conductivity of the sample.

Moreover,using pulsed EPR spectrometer we were able to study the dynamical properties of these photoexcited triplets as well as the interaction between the electron spin and ^{29}Si nuclear spin in the lattice. Finally we have demonstrated the coherent manipulation of ^{29}Si nuclear spin state via photoexcited triplet electron spin and show the coherent transfer of quantum information back and forth between the strongly hyperfine coupled triplet electrons and the nearest neighbor ^{29}Si nuclear spin, thus leading to the successful demonstration of ^{29}Si quantum memory in silicon.

1.4 Organization of thesis

Chapter 1 provides the motivation for the research presented in this thesis. This is followed with a general description of photoexcited triplet spin system. In addition, we introduce the triplet spin system in silicon relevant in this thesis.

Chapter 2 introduces the basics of magnetic resonance. In this chapter we discuss the fundamentals of pulsed EPR and EDMR techniques used in this thesis.

Chapter 3, 4 and 5 focuses on the main results of this thesis.

Chapter 3 discusses the electrical detection of spin dependent recombination process in phosphorus doped γ-irradiated silicon. First section of this chapter shows that with the introduction of these irradiation defects we can probe the spin state of phosphorus atoms in the bulk using EDMR spectroscopy, in contrast to the previous studies where paramagnetic centers situated near to the silicon surface can be probed using EDMR. Further we reveal that the dipolar interaction between triplets and phosphorus electron spin lead to the demonstration of electrical detection of cross relaxation signal in silicon. This new and sensitive method can also be used to probe paramagnetic centers in the lattice.

Chapter 4 is devoted to the pulsed EPR study of SL1 center in silicon. Here we have characterized the lifetime of the triplets as well as its interaction with the nearest neighbor ^{29}Si present in the lattice. It was found that all the triplet sublevels of SL1 centers were equally populated after the initial laser pulse. However, the different decay rates from the sublevels to the ground singlet state via spin-orbit coupling builds high spin polarization in these spin system. We use the electron spin echo envelope modulation spectroscopy to determine the hyperfine interaction with those ^{29}Si nuclear spin which are unresolved in the EPR spectrum.

In Chapter 5 we used the strong coupling of the SL1 center with the nearest neighbor ^{29}Si nuclear spins to demonstrate the Rabi oscillation of nuclear spins as well as the coherent transfer of quantum information between the electron and nuclear spin.

Chapter 6 summarizes the results obtained in this work.

Bibliography

[1] R. Feynman, Quantum mechanical computers. Opt. News **11**, 11-46 (1985). (Cited on page 1.)

[2] P. W. Shor, J. Sci. Stat. Comput, **26**, 1484 (1997). (Cited on page 1.)

[3] P. Domokos, J. M. Raimond, M. Brune, and S. Haroche , Phys. Rev. A, **52**, 3554 (1995). (Cited on page 1.)

[4] J. I. Cirac and P. Zoller, Phys. Rev. Lett., **74**, 4091 (1995). (Cited on page 1.)

[5] N. A. Gershenfeld and I. L. Chuang, Science, **275**, 350 (1997). (Cited on page 1.)

[6] N. H. Bonadeo,J. Erland, D. Gammon, D. Park, D. S. Katzer and D. G. Steel, Science, **282**, 1473 (1998). (Cited on page 2.)

[7] B. E. Kane, Nature, **393**, 133 (1998). (Cited on pages 2 and 3.)

[8] T. D. Ladd, J. R. Goldman, F. Yamaguchi, Y. Yamamoto, E. Abe, and K. M. Itoh, Phys. Rev. Lett. **89**, 017901 (2002). (Cited on pages 2 and 14.)

[9] K. M. Itoh, Solid State Commun. **133**, 747 (2005). (Cited on pages 2 and 14.)

[10] G. Feher, Phys. Rev. 114, 1219 (1959). (Cited on page 3.)

[11] J. J. L. Morton, A. M. Tyryshkin, R. M. Brown, S. Shankar, B. W. Lovett, A. Ardavan, T. Schenkel, E. E. Haller, J. W. Ager and S. A. Lyon, Nature, **455**, 1085 (2008). (Cited on page 4.)

[12] A.M. Tyryshkin, S. A. Lyon, A. V. Astashkin, and A. M. Raitsimring, Phys. Rev. B **68**, 193207 (2003). (Cited on page 4.)

[13] S. Simmons, R. M. Brown, H. Riemann, N. V. Abrosimov, P. Becker, H. J. Pohl, M. L. W. Thewalt, K. M. Itoh and J. J. L. Morton, Nature **470** 69 (2011). (Cited on page 4.)

[14] E. Hahn, Phys. Rev. B. **80**, 460 (1946). (Cited on page 5.)

[15] A. E. Dementyev, D. Li, K. MacLean, and S. E. Barrett, Phys. Rev. B **68**, 153302 (2003). (Cited on page 5.)

[16] T. D. Ladd, D. Maryenko, Y. Yamamoto, E. Abe, and K. M. Itoh, Phys. Rev. B **71**, 014401 (2005). (Cited on pages 5 and 14.)

[17] G. Lampel, Phys. Rev. Lett., **20**, 491 (1968). (Cited on page 5.)

[18] A. S. Verhulst, I. G. Rau, Y. Yamamoto and K. M. Itoh, Phys. Rev. B, **71**, 235206 (2005). (Cited on page 5.)

[19] H. Hayashi, T. Itahashi, K. M. Itoh, L. S. Vlasenko, and M. P. Vlasenko, Phys. Rev. B **80**, 045201 (2009). (Cited on page 5.)

[20] A. E. Dementyev, D. G. Cory and C. Ramanathan, J. Chem. Phys. **134**, 154511 (2011). (Cited on page 5.)

[21] J.H.van der Waals, Appl. Magn. Reson. **20**, 545 (2001). (Cited on pages 9 and 10.)

[22] M. Deimling, H. Brunner, K. P. Dinse, K. H. Hausser, and J. P. Colpa, J. Magn. Reson. **39**, 185 (1980). (Cited on pages 9 and 10.)

[23] S. P. McGlynn, T. Azumi, M. Kinosita, Molecular spectroscopy of the triplet state, Prentice-Hall, Englewood Cliffs, NJ (1969). (Cited on page 9.)

[24] J. Wrachtrup, C. von Borczyskowski, J. Bernard, M. Orritt and R. Brown, Nature **363**, 244 (1993). (Cited on page 10.)

[25] T. Chin Yang, D. J. Sloop, S. I. Weissman and T. Sung Lin , J. Chem. Phys. **113**, 11194 (2000). (Cited on page 10.)

[26] P. Bachert, H. Brunner, K. H. Hausser, and J. P. Colpa, Chem. Phys. **91**, 435 (1984). (Cited on page 10.)

[27] K. Takeda, K. Takegoshi and T. Terao, J. Phys. Soc. Japan **73**, 2319 (2004). (Cited on page 10.)

[28] J. Schmidt, D. J. van den Heuvel, A. Henstra, T.-S. Lin and W. Wenckebach, Pure & App. Chem. **64**, 859 (1992). (Cited on page 10.)

[29] M. Schaffry, V.Filidou, S. D. Karlen, E. M. Gauger, S. C. Benjamin, H. L. Anderson, A. Ardavan, G. A. D. Briggs, K. Maeda, K. B. Henbest, F. Giustino, J. J. L. Morton and B. W. Lovett, Phys. Rev. Lett. **104**, 200501 (2010). (Cited on page 10.)

[30] V.Filidou, S. Simmons, S. D. Karlen, H. L. Anderson, F. Giustino, J. J. L. Morton *in preparation* (2011). (Cited on page 10.)

[31] A. M. Stoneham, A.J. Fischer and P. T. Greenland, J. Phys. Cond. Mat. **15**, L447 (2003). (Cited on page 10.)

[32] A. V. Yukhnevich, Sov. Phys.-Solid State, **7**, 259 (1965). (Cited on page 12.)

[33] G. D. Watkins, J. W. Corbett and R. M. Walker, J. Appl. Phys **30**, 1198 (1959). (Cited on page 12.)

[34] G. D. Watkins and J. W. Corbett, Phys. Rev. **121**, 1001 (1961). (Cited on page 12.)

[35] J. W. Corbett, G. D. Watkins, R. M. Chrenko and R. S. McDonald, Phys. Rev. **121**, 1015 (1961). (Cited on page 12.)

[36] F.A. Abou-el-Fotouh and R.C. Newman, Sol. State Commun. **15**, 1409 (1974). (Cited on page 12.)

[37] K. L. Brower, Phys. Rev. B **4**, 1968 (1971). (Cited on pages 12 and 13.)

[38] L. S. Vlasenko, Yu. V. Martynov, T. Gregorkiewicz, and C. A. J. Ammerlaan, Phys. Rev. B **52**, 1144 (1995). (Cited on page 12.)

[39] L. S. Vlasenko, M. P. Vlasenko, D. S. Poloskin, R. Laiho, H. Hayashi, T. Itahashi, A. Sagara, and K. M. Itoh, Phys. Stat. Sol. (c). **3**, 12 (2006). (Cited on page 14.)

[40] T. Itahashi, H. Hayashi, K.M. Itoh, D.S. Poloskin, and L.S. Vlasenko, Physica B **404**, 5054 (2009). (Cited on page 14.)

[41] F. Jelezko, T. Gaebel, I. Popa, M. Domhan, A. Gruber, and J.Wrachtrup, Phys. Rev. Lett. **93**, 130501 2004 (Cited on page 14.)

[42] M. V. Gurudev Dutt, L. Childress, L. Jiang, E. Togan, J. Maze, F. Jelezko, A. S. Zibrov, P. R. Hemmer, and M. D. Lukin, Science **316**, 1312 (2007). (Cited on page 14.)

[43] P. Neumann, N. Mizuochi, F. Rempp, P. Hemmer, H. Watanabe, S. Yamasaki, V. Jacques, T. Gaebel, F. Jelezko, and J. Wrachtrup, Science **320**, 1326 2008 (Cited on page 14.)

Chapter 2

Magnetic Resonance

Ever since the first experimental observation of an electron paramagnetic resonance (EPR) signal by E. K. Zavoisky at Kazan State University, Russia, the EPR spectroscopy has made a great contribution for determining the structure and dynamics and the spatial distribution of paramagnetic species in host materials. The development of pulsed EPR (pEPR) and electrical detection of magnetic resonance (EDMR) spectroscopy had further enriched the field of magnetic resonance and its contribution towards understanding atomic physics. In this chapter we discuss the basic understanding of the underlying theory and fundamentals of these magnetic resonance techniques utilized in this thesis.

2.1 Introduction

2.1.1 Electron magnetic moment and its interaction with magnetic field

From classical electrodynamics, a rotating electrically charged body creates a magnetic dipole with magnetic poles of equal magnitude but opposite polarity. If the electron is visualized as a classical charged particle literally rotating about an axis with angular momentum **J** , its magnetic dipole moment μ is given by:

$$\mu = \gamma \mathbf{J}, \tag{2.1}$$

where γ is the gyromagnetic ratio. Thus, an electron can be considered as a tiny bar magnet and an application of static magnetic field B will exert a torque equal to the time derivative of the angular momentum:

$$\frac{d\mathbf{J}}{dt} = \mu \times \mathbf{B}, \tag{2.2}$$

Using Eqn. 2.1 , we re-write Eqn. 2.2 as:

$$\frac{d\mu}{dt} = \mu \times \gamma \mathbf{B}, \tag{2.3}$$

The above equation illustrates that the magnetic moment precess about the magnetic field as shown in Figure 2.1. If the applied static magnetic field is along the z-axis, i.e. $\mathbf{B} = B_0\hat{z}$, the magnetic moment μ rotates at an angular frequency $\omega_0 = \mid \gamma \mid B_0$ [1]. The angular frequency is also known as Larmour frequency.

The magnetic moment also takes on a potential energy **U** in the presence of magnetic field **B** which is given as,

$$\mathbf{U} = -\mu.\mathbf{B} \tag{2.4}$$

Quantum mechanics predicts that the angular momentum **J** can take only some discrete sets of value. i.e. quantization of angular momentum. We introduce an quantum operator **I**, such that **J**=$\hbar$ **I**. $\mathbf{I}^2$ has eigenvalues $I(I+1)$, where I is either integer or half integer. Any component of **I** (for example $\mathbf{I}_z$) commutes with $\mathbf{I}^2$, so we can specify simultaneous eigenvalues of both I^2 and I_z. Let m be the eigenvalue of $\mathbf{I}_z$ which may take any of the $2I$+1 values I,I-1,$\cdots$ -I. Considering this fact, the Hamiltonian of the electron in the presence of the magnetic field is given by equation

$$\mathcal{H} = -\mu.\mathbf{B}, \tag{2.5}$$

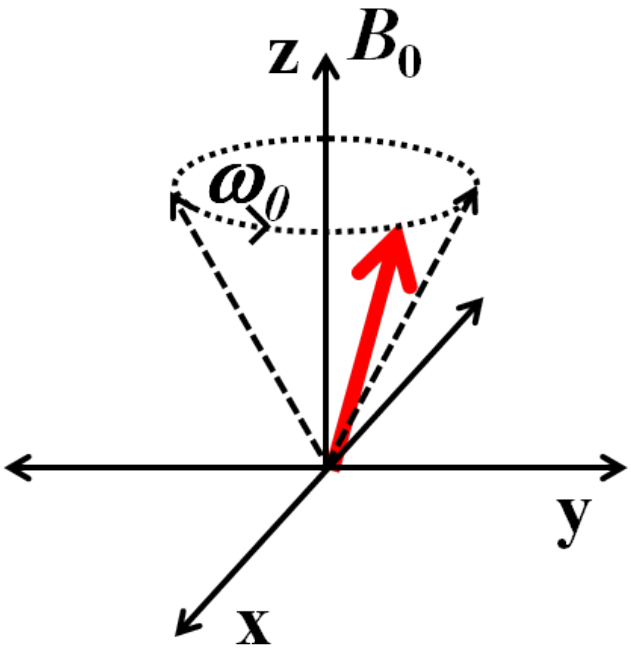

Figure 2.1: Larmor Frequency - Schematic showing the precession of the magnetic moment in the presence of externally applied magnetic field.

With magnetic field taken along $\hat{z}$ -direction ,

$$\mathcal{H} = -\gamma\hbar B_0 \mathbf{I_z}, \tag{2.6}$$

The eigenvalue of this Hamiltonian is simple, E=-$\gamma\hbar$B$_0 m$, where m=$I, I-1, \cdots, -I$. For spin-1/2 particle (**I**=1/2), the angular momentum along the $\hat{z}$-axis has two eigenstates, $|\alpha\rangle$ and $|\beta\rangle$. These states are defined as $|\alpha\rangle = |1/2, +1/2\rangle$ and $|\beta\rangle = |1/2, -1/2\rangle$ using the notation $|I, m\rangle$. The states $|\alpha\rangle$ and $|\beta\rangle$ are called the Zeeman eigenstates of the single spin-1/2 and obey the following eigenequation:

$$\mathbf{I_z}\,|\alpha\rangle = +1/2\,|\alpha\rangle\,, \mathbf{I_z}\,|\beta\rangle = -1/2\,|\beta\rangle \tag{2.7}$$

Using Eqn. 2.6 and 2.7, the eigen energy of the state $|\alpha\rangle$ and $|\beta\rangle$ is computed to be -$\hbar\omega_0/2$ and $\hbar\omega_0/2$, respectively. The state $|\alpha\rangle$ has lower energy, meaning it is parallel to the magnetic field while the state $|\beta\rangle$ is antiparallel to the magnetic field. The energy difference between the states is $\hbar\omega_0$ and thus any transition between these states must involve energy quanta $\hbar\omega_0$. The required energy corresponds exactly to the Larmor frequency, giving rise to the concept of “resonance".

2.1.1.1 Effect of alternating magnetic field

In this section we will consider the effect of alternating magnetic field (microwave field) on the magnetic moment. Let's consider the situation in which, in addition to the static magnetic field B_0 along $\hat{z}$-axis, an external perpendicular alternating magnetic field $B_x \cos(\Omega t)\hat{x}$ is applied. This linearly polarized microwave field can be decomposed into right and left circularly polarized microwave fields in the xy-plane. In the rotating wave approximation, only the right-circularly polarized field ($\mathbf{B_1}(t) = B_1(\hat{x}\cos(\Omega t) + \hat{y}\sin(\Omega t))$) effects the magnetic moment near the resonance condition $\Omega \simeq \omega_0$ and the effect of the left-circularly polarized field may be neglected because it is far off-resonance. The equation of motion of the magnetic moment can now be written as

$$\frac{d\mu}{dt} = \mu \times \gamma(B_1(\hat{x}\cos(\Omega t) + \hat{y}\sin(\Omega t)) + B_0\hat{z}), \tag{2.8}$$

The time dependence of $\mathbf{B_1}$ field adds to the complexity of solving the above equation of motion. However, the time dependence can be removed if we consider a coordinate system rotating at an angular frequency Ω. From this rotating frame, $\mathbf{B_1}$ is stationary and thus Eqn. 2.8 can be re-written as

$$\frac{d\mu}{dt} = \mu \times \gamma(B_1\hat{x'} + (B_0 - \Omega/\gamma)\hat{z'}), \tag{2.9}$$

Therefore the magnetic moment is subjected to a precession about the effective magnetic field, $\mathbf{B}_{eff} = B_1\hat{x'} + B_0 - \Omega/\gamma\hat{z'}$. Thus, beside the stationary $\mathbf{B_1}$,the magnetic field along the z′-axis that coincides with the z-axis of the laboratory frame is reduced from B_0 to $B_0 - \Omega/\gamma$. If the resonance condition is fulfilled exactly ($\Omega = \gamma B_0$), the effective field is then simply $\hat{x'}B_1$. The magnetic moment will then precess in the y-z plane remaining parallel to $\mathbf{B_1}$. The rotation frequency $\omega_1 = \gamma B_1$, is called the Rabi oscillation.

By turning the alternating field on and off at proper timings, we are able to control the precession angle (θ) of the magnetic moment, i.e., $\theta = \gamma B_1 t_w$, where t_w is the duration of the alternating field. If t_w is chosen such that $\theta = \pi$, the pulse would simply invert the magnetic moment. Such a pulse in literature is defined as π-pulse, similarly we can define a $\pi/2$-pulse.

So far we only considered single spin interacting only with the magnetic field. However, in reality a sample contains large number of identical spins and is not isolated from various interaction in the lattice. The macroscopic magnetization $\mathbf{M}$ is a vector sum of all the individual magnetic moments in the sample, and for a large enough number of spins the x-y component will cancel out and the resultant net magnetization will be

along the +z axis and exactly parallel to the external field. Thus, in thermal equilibrium, we write the equilibrium magnetization as $M_{eq} = (0, 0, M_0)$. Now, if the system of spin is not in thermal equilibrium than under various interaction the magnetization reaches M_{eq} , which could be explained by the Bloch equation [2]:

$$\frac{d\boldsymbol{M}}{dt} = \boldsymbol{M} \times \gamma \ \boldsymbol{B} + \frac{1}{T_1}(\boldsymbol{M}_{eq} - \boldsymbol{M}_{\parallel}) - \frac{1}{T_2} \ \boldsymbol{M}_{\perp}, \tag{2.10}$$

where $\boldsymbol{M}_{\parallel}$ and $\boldsymbol{M}_{\perp}$ are the longitudinal and transverse component of magnetization $\boldsymbol{M}$ and T_1 , T_2 are the relaxation processes. Once disturbed from its equilibrium, the magnetization will interact with its surroundings and return to equilibrium. This process is called relaxation, and is characterized by two time constants, T_1 and T_2. The spin-lattice relaxation time, T_1, describes how quickly the magnetization recovers its longitudinal component along the z axis, in other words, it is the amount of time in which the energy absorbed from the pulse is dissipated to the lattice as the system returns to equilibrium. The transverse relaxation time, T_2, describes how quickly the net magnetization dissipates in the x-y plane, i.e. how quickly the spins lose coherence and fan out 360 degrees into randomized precession.

2.2 Pulsed Electron Paramagnetic Resonance

The heart of pulse EPR experiments lies in the manipulation of the magnetization by short and intense microwave pulses that have specific tip angles, and then the subsequent detection of the magnetic behavior during its return to equilibrium. Pulses are often named by their tip angles, and the most commonly employed tip angles are $\pi/2$ (90 degrees) and π (180 degrees). A $\pi/2$ pulse will tip the magnetization into the x-y plane, and is also called a saturating pulse because the magnetization along the z axis goes to zero, i.e. the population difference between parallel and antiparallel states goes to zero. A π pulse is also called an inversion pulse, because it tips the magnetization 180 degrees. Using well defined pulse sequences we can measure the various relaxation process like T_1 and T_2 time.

The simplest way to measure the T_2, would be to apply a $\pi/2$ pulse which will tip the magnetization in the x-y plane and then monitor the decay of magnetization with time. However, in reality the spin ensemble do not have the same Larmor frequency due to the inhomogeniety in the magnetic field and thus the transverse magnetization tends to fan out in the x-y plane at time scale faster than T_2. The magnetic field inhomogeneity (δB_z) arises as external magnetic field (B_0) is not homogeneous over sample volume and also because of the presence of other paramagnetic centers which creates local magnetic field. As a result of this, the Larmor frequency of the spins is shifted by $\delta\omega = \mid \gamma\delta B_z \mid$. A spin packet in a pEPR represents a group of spins having same Larmor frequency. As seen from the frame rotating at an angular frequency ω_0, the spin packet precess at at angular frequency $\delta\omega$. The magnetization vector is composed of many spin packets which are precessing with different angular frequency and the magnetization vector vanishes as it fan out over the entire x-y plane. This is called a Free Induction Decay (FID). Thus to measure the T_2 time we need to overcome the effect of inhomogeneity. This can be achieved by using a Hahn echo pulse sequence [3] .

2.2.1 Hahn echo method

The basic idea of the Hahn echo method is to overcome the unwanted decay of the transverse magnetization due to the magnetic field inhomogeneity. The pulse sequence employed is $\pi/2 - \tau - \pi - \tau - echo$. The first $\pi/2$ pulse will bring the magnetization in the x-y plane where the magnetization evolves over the time τ. As mentioned above, if we look down the z axis at the x-y plane, there will be faster moving spin packets and slower moving spin packets, depending on their relative frequencies. When we apply a

π pulse, the magnetization is inverted 180 degrees yet still rotates in the same direction with the same speed. Now, instead of moving away from the slower spin packets, the faster moving spin packets move towards the slower spin packets. The magnetization eventually refocuses at time τ after the π pulse to form an echo. The echo intensity as a function of waiting time τ will eventually gives us the T_2 time of the spin system under observation. Figure 2.2 is the pictorial representation of the Hahn echo method describing the effect of pulse sequences on the spins.

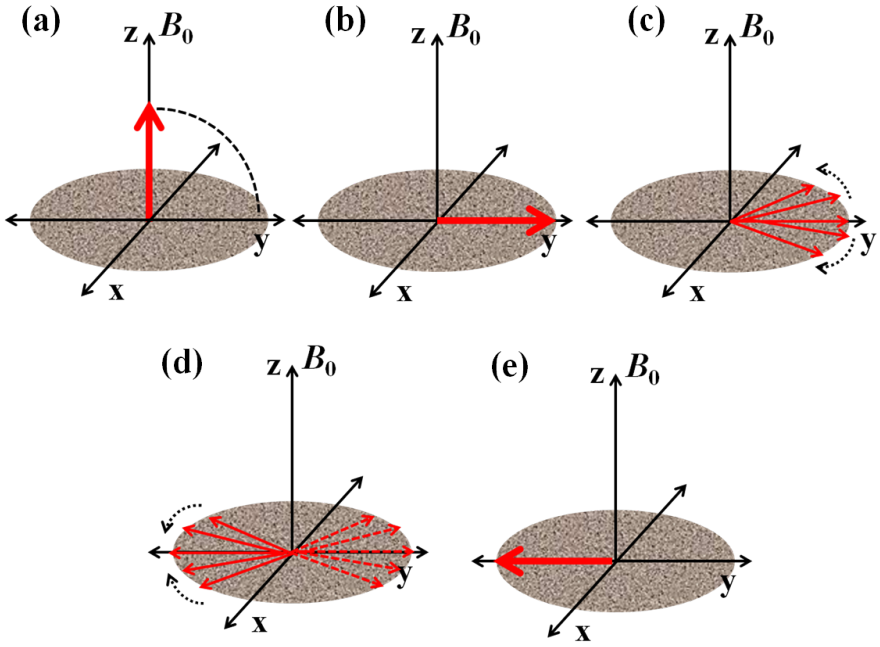

Figure 2.2: Hahn Echo - Schematic showing the spin behavior under the application of Hahn echo pulse sequence. (a) Initialization of spin along the applied magnetic field, which under the application of $\pi/2$ pulse goes to the x-y plane(b). (c) Dephasing of spins in the x-y plane which is refocused using the π pulse (d). (e) The occurence of echo as the spins get refocused.

2.2.2 Spin-Spin Interaction

The other advantage of pEPR is to study the interaction of paramagnetic centers with nuclear spins in the lattice. The paramagnetic centers in solid generally interacts with more than one nuclear spin which inhomogeneously broadens the EPR spectrum (Figure 2.3 (a)). Because of this poor resolution in cw-EPR, many magnetic parameters essential for the characterization of the paramagnetic centers can not be addressed. A

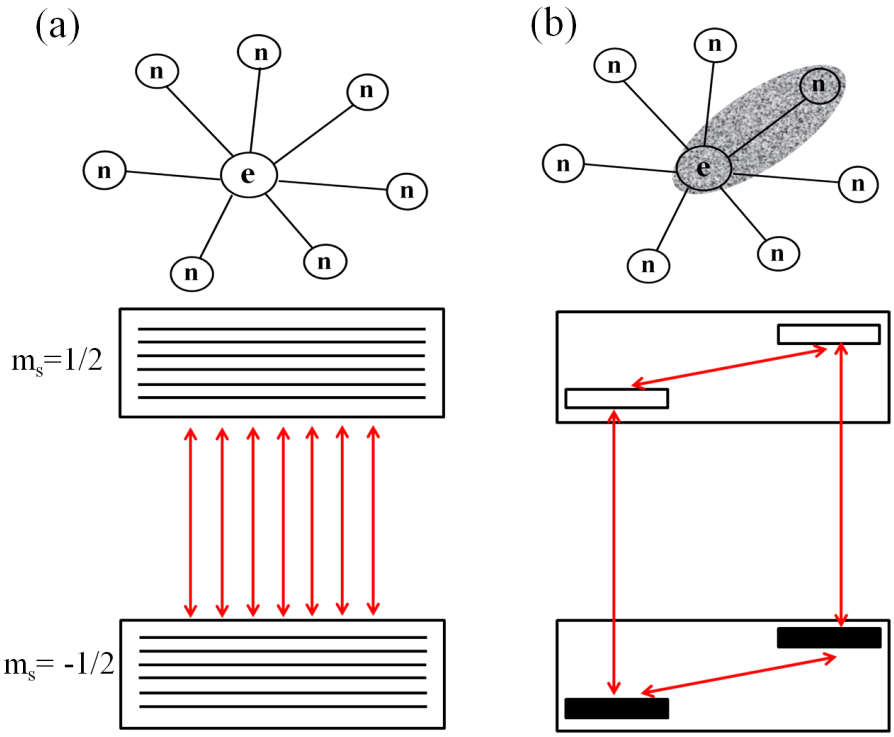

Figure 2.3: Coupled electron-nuclear spin system - (a) Multi-spin system: the elctron spin interacting with many nuclear spins to give an EPR spectrum consisting of a large number of transition. (b) Two-spin subsystem: only the interaction of the electron spin with one nuclear spin, $I = 1/2$, is considered. The EPR spectrum of such a subsystem consists of two (allowed) transitions.

way out for this is to use pulse EPR method, which can be use to address subsystem of a multi-spin system. Figure 2.3(b) shows the spin system consisting of one electron and one nuclear spin. The rotating-frame spin Hamiltonian of such a two-spin subsystem is given by

$$\mathcal{H}_0 = \Omega_s S_z + \omega_I I_z + \boldsymbol{I}\mathbf{A}\mathbf{S}, \tag{2.11}$$

where $\Omega_s = \omega_s$ - ω_{mw}, $\mathbf{A}$ is the hyperfine coupling tensor, ω_s=γ_eB$_0$ and ω_I=γ_IB$_0$. The two allowed (Δm$_s$=$\pm$1, Δm$_I$=0) and two forbidden (Δm$_s$=$\pm$1, Δm$_I$=$\pm$1) electron spin transition frequencies in the rotating frame can be expressed as

$$\omega_{13} = \Omega_s + \frac{1}{2}(\omega_{12} - \omega_{34}), \tag{2.12}$$

$$\omega_{24} = \Omega_s - \frac{1}{2}(\omega_{12} - \omega_{34}), \tag{2.13}$$

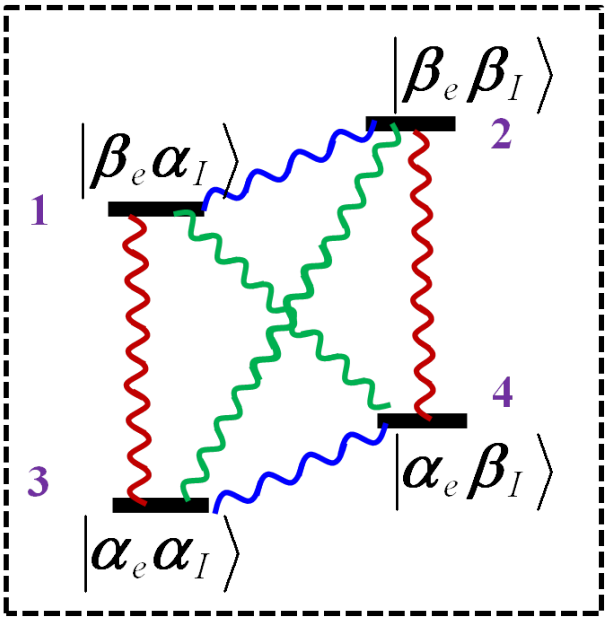

Figure 2.4: Coherences in four level system - Schematic showing the four level system consisting of hyperfine coupled electron spin $S = 1/2$ and nuclear spin $I = 1/2$. The zig-zag lines represent the various possible coherences that can be generated under the application of resonant microwave and radio frequency pulse.

and

$$\omega_{14} = \Omega_s + \frac{1}{2}(\omega_{12} + \omega_{34}), \tag{2.14}$$

$$\omega_{23} = \Omega_s - \frac{1}{2}(\omega_{12} + \omega_{34}), \tag{2.15}$$

with the two nuclear transition frequencies, also know as "electron nuclear double resonance(ENDOR)" frequencies given as

$$\omega_\alpha = \Omega_{12} = [(m_s A + \omega_I)^2 + (m_s B)^2]^{1/2}, \tag{2.16}$$

$$\omega_\beta = \Omega_{34} = [(m_s A - \omega_I)^2 + (m_s B)^2]^{1/2} \tag{2.17}$$

Figure 2.4 shows coherence associated with the electron (allowed and forbidden transition) and nuclear transition. pEPR gives the experimental tool to address such coherences to measure the T_2 and T_1 time of the coupled electron and nuclear spin system.

2.3 Electrically detected magnetic resonance

The sensitivity limit of EPR can be overcome by applying electrically detected magnetic resonance (EDMR) to study paramagnetic centres in semiconductors. This technique combines the microscopic selectivity of EPR with the sensitivity of a current measurement and thus provides a tool to directly study the influence of paramagnetic defects on the conductivity. EDMR was demonstrated in 1966 by Maxwell and Honig [4, 5] as well as Schmidt and Solomon [6] who measured the influence of EPR on the photoconductivity in silicon. The underlying mechanism was spin-dependent scattering of charge carriers at impurities. In 1972 Lepine utilized EDMR for the detection of charge carrier recombination via defect states at a silicon surface [7]. Since then, EDMR was applied to a large variety of inorganic and organic semiconductors.

The “spin-to-charge" mechanisms for the effects studied in this thesis are spin-dependent recombination processes that rely on the spin-pair mechanism developed by Kaplan, Solomon and Mott which is referred to as the KSM model [8]. Two electrons occupy two localized states in close proximity and constitute a spin pair as shown in Figure 2.5.

Although it would be energetically favourable if both electrons occupied the lower-lying state, however due to the Pauli-principle this transition is only allowed when both spins are aligned antiparallel. The application of microwave (mw) radiation, which is resonant with either of the two spin pair, alters the respective spin state and the initially forbidden transition becomes allowed. The recombination process is then completed by the capture of a hole from the valence band. In addition, an electron from the conduction band can be trapped at unoccupied defect state. All in all, one electron from the conduction band and one hole from the valence band are annihilated, resulting in a decrease of the sample conductivity.

EDMR experiments are performed similar to continuous wave (cw) EPR experiments, i.e. the sample was continuously subjected to microwave radiation while sweeping an external magnetic field and detecting the photoconductivity. However, in contrast to cw-EPR, the EDMR signal is independent of applied magnetic field and it achieves maximum intensity under intense microwave or rf field to saturate the energy levels.

The EDMR signal intensity is independent of the applied magnetic field, so in this thesis we have used low field EDMR setup which allows us to experimentally observe some high field forbidden transitions. In the low field regime we can not ignore the hyperfine term and that leads to mixing of states. Phosphorus eigenstates (see section

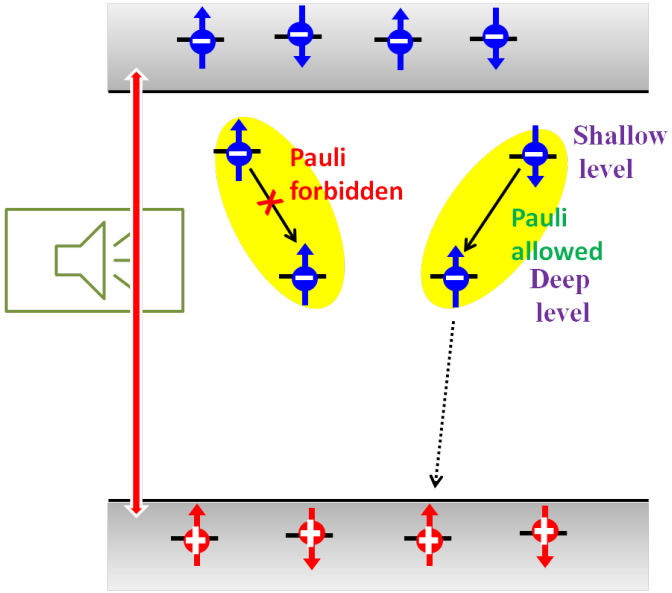

Figure 2.5: KSM Model - A donor(shallow level)-acceptor (deep level) model to explain the spin dependent recombination. The spin pairs of shallow and deep level paramagnetic centers in the triplet state does not recombine while those in spin singlet recombine on a much faster time scale. Thus under steady state condition most of the spin pairs are in spin triplet. Under application of resonant oscillating magnetic field we can flip one of the spin to change the configuration from spin triplet to the singlet state and thus enhancing the recombination which changes the photoconductivity of the sample.

1.1.2) in the low field regime are given by;

$$|1\rangle = |\uparrow\uparrow\rangle\,, \tag{2.18}$$

$$|2\rangle = \alpha\,|\uparrow\downarrow\rangle + \beta\,|\downarrow\uparrow\rangle\,, \tag{2.19}$$

$$|3\rangle = -\beta\,|\uparrow\downarrow\rangle + \alpha\,|\downarrow\uparrow\rangle\,, \tag{2.20}$$

$$|4\rangle = |\downarrow\downarrow\rangle\,, \tag{2.21}$$

where α ,β represents the mixing coefficient. Such superposition states has been characterized using low field EDMR previously [9]. Figure 2.6 shows the low-field EDMR setup used in this work. As EDMR signal is independent of magnetic field, it allowed us to observe magnetic resonance of paramagnetic centers in low magnetic field.

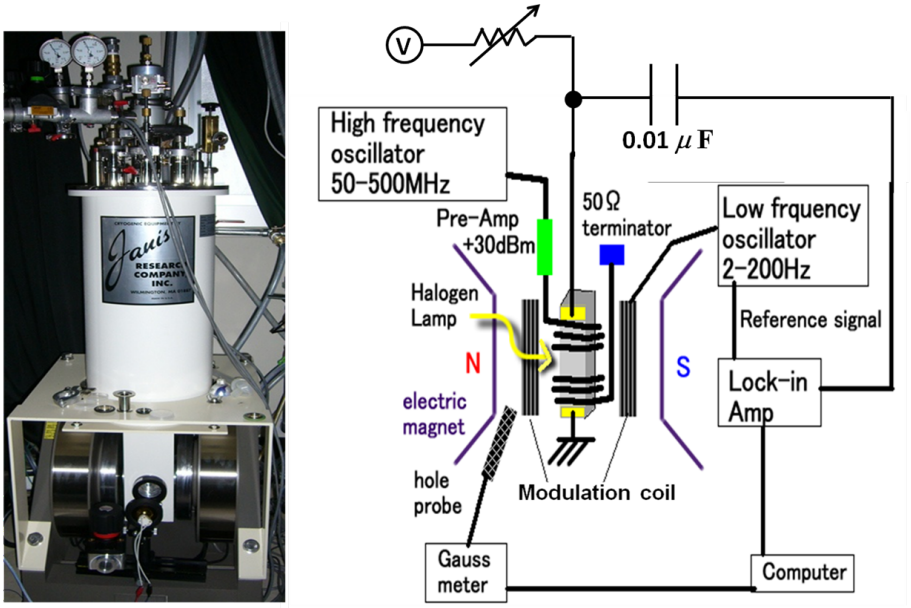

Figure 2.6: Low field EDMR setup - Cryostat and the electrical circuit used to realize low field EDMR setup used in this work [10].

Bibliography

[1] C. P. Slichter, Principles of Magnetic Resonance, Springer (1966). (Cited on page 21.)

[2] F. Bloch, Phys. Rev. B. **70**, 460 (1946). (Cited on page 24.)

[3] E. Hahn, Phys. Rev. B. **80**, 460 (1946). (Cited on page 25.)

[4] A. Honig, Phys. Rev. Lett. **17**, 186 (1966). (Cited on page 29.)

[5] R. Maxwell and A. Honig, Phys. Rev. Lett. **17**, 188 (1966). (Cited on page 29.)

[6] J. Schmidt and I. Solomon, Compt. Rend. Acad. Sci. B. **263**, 169 (1966). (Cited on page 29.)

[7] D. J. Lepine, Phys. Rev. B. **6**, 436 (1973). (Cited on page 29.)

[8] D. Kaplan, I. Solomon and N. F. Mott, J. Phys. Lett. **39**, L51 (1978). (Cited on page 29.)

[9] H. Morishita, L. S. Vlasenko, H. Tanaka, K. Semba, K. Sawano, Y. Shiraki, M. Eto and K. M. Itoh, Phys. Rev. B **80**, 205206 (2009). (Cited on page 30.)

[10] H. Morishita, "Characterization of phosphorus donors n silicon by low magnetic field electrically detected magnetic resonance", PhD Thesis (2011) (Cited on page 31.)

Chapter 3

Spin dependent recombination processes in phosphorus doped γ-irradiated silicon

---

In this chapter, we will explain various spin dependent recombination processes in silicon that can be used to probe paramagnetic centers in silicon. The first part of the chapter is on the electrically detected magnetic resonance where the photoconductivity is monitored under the scanning magnetic filed with application of oscillating magnetic field. The latter part is about the cross relaxation process in the bulk of the sample when two different electron species are present. These are very sensitive methods and could be used to probe variety of defects in semiconductor.

3.1 Electrically detected magnetic resonance

Electrically detected magnetic resonance (EDMR) of phosphorus in silicon was detected in weak magnetic fields at low resonance frequencies of 200 MHz - 400 MHz before and after irradiation of Cz-grown silicon samples by γ-rays. EDMR spectra were detected by measuring dc-photoconductivity of samples under band-gap illumination. Phosphorus (P^0) EDMR lines are always accompanied with the single line(S-line) with g-factor 2.01 originated most likely from the surface recombination centers. Significant enhancement in the P^0 and S-line EDMR signals was found in the same samples after irradiation with the doses of (3-6)$\times 10^{15}$ γ/cm^2. For these doses of irradiation we were also able to see the ESR transition between entangled states of phosphorous formed at low magnetic field. This shows the higher efficiency of spin dependent recombination (SDR) process in irradiated samples. In addition, several new EDMR lines emerged after irradiation. Some of them arose from the spin dependent recombination through the photoexcited triplet states of A-centers (oxygen+vacancy complex).

3.1.1 Introduction

Electrically detected magnetic resonance (EDMR) is a powerful and sensitive method for investigating spin dependent recombination (SDR) processes involving different recombination centers in semiconductors. The change in conductivity and photoconductivity of silicon under magnetic resonance of phosphorus (P^0) donors was observed and investigated many years ago [1]. It was argued that the processes of spin dependent scattering of the conducting electrons from paramagnetic donor centers [2] and spin dependent capture of electrons by neutral shallow donors [3] are responsible for the change in conductivity under magnetic resonance. Suggested mechanisms of spin dependent conductivity require high electron spin polarization achieved at low temperatures below 4.2 K and strong magnetic fields used in standard electron paramagnetic resonance (EPR) spectrometer.

Ever-since the observation of SDR effect in silicon at room temperature, reported by Lepine [4], many experimental and theoretical investigations of SDR were performed which showed the independence or weak dependence of EDMR signals on the magnetic field strength. These experimental results were well explained by the SDR model, (donor-acceptor recombination process) developed by Kaplan, Solomon and Mott [5] were they consider small but finite exchange-interaction between electron spin pairs in the triplet spin S=1 state before they recombine to bring change in the photoconductivity.

EDMR spectroscopy provide the opportunity to observe EPR signals of recombination centers in small samples with electrical contacts. In addition, complementary information concerning the properties of paramagnetic centers and SDR processes can be obtained from the EPR spectra in weak magnetic fields because the additional EDMR lines due to the mixing of spin states, magnetic level crossing, and anticrossing can be observed. The first low frequency observation of EDMR spectra of P^0 centers and of the excited spin S=1 states of the neutral A-centers (oxygen+vacancy complex) in low dose irradiated silicon has been reported in Ref [6]. An additional line with g-factor g≈2 was observed but not identified at that time. Similar EDMR spectra were observed in irradiated and post annealed samples almost 8 years later [7] and it was pointed out that no EDMR spectra of shallow donors were observed in as-grown n-type silicon and that the g≈2 line originated from thermal donors and A-centers.

In the present paper we report the results of experimental detection of EDMR signals in weak magnetic fields monitoring the change in dc-photoconductivity of silicon samples under magnetic resonance. We also report the effects of etching the samples with hydro-

fluoric acid(HF)and γ-irradiation on the EDMR signal of phosphorous atoms in silicon.

3.1.2 Experimental

Ohmic contacts for the EDMR measurement were made by ion-implantation and post-implantation annealing of arsenic on silicon wafers doped with phosphorous(1×10^{15}cm^3). Samples were irradiated by γ-rays emitted from a ^{60}Co source at room temperature with the dose of irradiation from 10^{14} to 6×10^{15}cm^{-2}. The EDMR measurements were performed at low magnetic field $B_0 \leq 50$ mT with B $\parallel \langle 110 \rangle$ and at temperature between 6-20 K.Radio frequency used for the measurement was applied by a coil wrapped around the sample. 100 W halogen lamp was used for creating photoexcited carriers. Prior to each measurement, the surface oxide was removed with dilute hydro-fluoric acid(HF) solution to reduce the concentration of surface defects. A lock-in-detector tuned to the second harmonic of magnetic field modulation frequency of 2 KHz was employed to increase the signal to noise ratio. The EDMR signals were recorded as a second derivative of the magnetic field.

3.1.3 Results and discussions

EDMR spectra observed with the resonance frequency of 200 MHz in a Si sample before and after γ-irradiation are shown in Figure 3.1. The positive sign of signals corresponds to the increase of the recombination rate and decrease of photoconductivity in the sample.

The EDMR spectrum of phosphorus donor atoms is detected together with the line labeled S-line (surface recombination center)with g-factor about 2.01. In non-irradiated sample, the intensity of S-line decreases together with the intensity of phosphorus lines when the surface oxide was removed with HF. This allows us to conclude that S-line arises from the surface recombination centers and SDR process includes the spin dependent electron transfer from phosphorus to surface paramagnetic centers. This is consistent with the previous report where EDMR of phosphorous in silicon has been attributed to the spin dependent recombination between neutral donor(P^0) and paramagnetic states at the Si/SiO_2 interface [23]. Figure 3.1 also shows the EDMR spectrum from the sample after γ irradiation. The increase of about 10 times in EDMR intensity of the P^0 and S-line is observed for the irradiation doses of (3-6)$\times10^{15}$ cm^{-2}. The concentration of radiation defects created in silicon by γ-rays at these doses of irradiation cannot exceed 10^{14} cm^{-2}. At higher doses of irradiation the intensity of the

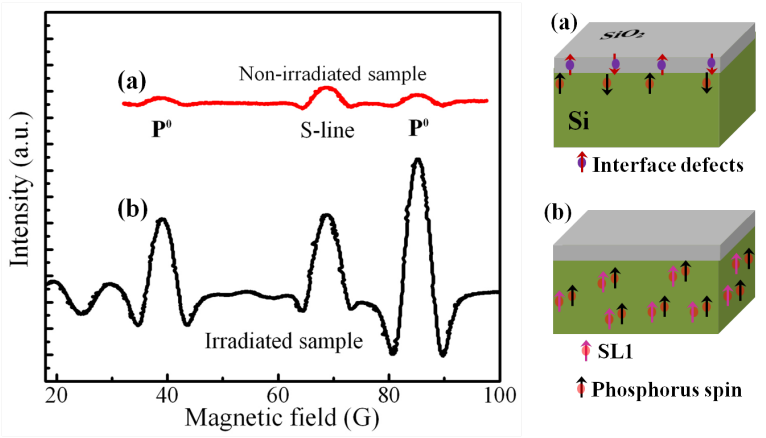

Figure 3.1: Effect of γ-irradiation on EDMR signal - EDMR signal and pictorial representation of SDR : (a) at the surface for non-irradiated sample and (b) in the bulk for irradiated sample. The signal is measured as a function of magnetic field with an applied constant RF of 200 MHz at temperature T=7 K.

P^0 EDMR lines decreases. The increase in the efficiency of SDR process after irradiation can be attributed to the increase of radiation defects that take electrons away from phosphorus donors increasing the concentration of positively charged phosphorus atoms being effective capture centers of photoexcited electrons increasing the efficiency of the spin dependent recombination process. Also,the spin dependent transfer of the captured electrons from phosphorus to another radiation defects localized near phosphorus atoms can increase the efficiency of SDR in bulk of the sample. Unlike the case for the surface centers serving exclusively as spin dependent recombination centers,the recombination centers created by the γ-ray are distributed uniformly through out the bulk sample. Therefore,the SDR occurs not only near the surface but throughout the bulk region leading to much larger change in the conductivity. Figure 3.2 compares the EDMR spectra of the irradiated sample with and without the surface oxide layer.

Here the decrease of S-line intensity observed after the etching is attributed to the reduction in the surface recombination centers. However,the EDMR signal intensity of phosphorous remains unchanged showing that the SDR is occurring throughout the bulk region. Figure 3.3 shows the EDMR spectrum from irradiated sample at lower modulation frequency(1KHz). We can observe an additional EDMR signal,marked by an arrow in Figure 3.3, which is not visible for non-irradiated samples doped with phosphorous.This signal is due to the transition between the superposition states of phosphorous formed at low magnetic field. Inset in Figure 3.3 shows the phosphorous

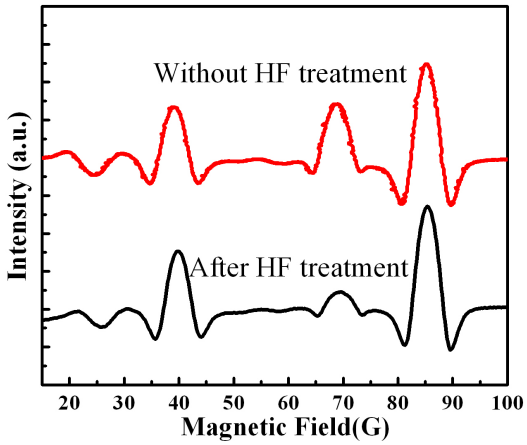

Figure 3.2: Effect of HF treatment on EDMR signal from γ-irradiated silicon - EDMR spectra detected in irradiated sample before and after HF treatment. The removal of oxide layer by HF has no significant effect on phosphorus signal. The signal was measured with an applied RF of 200 MHz.

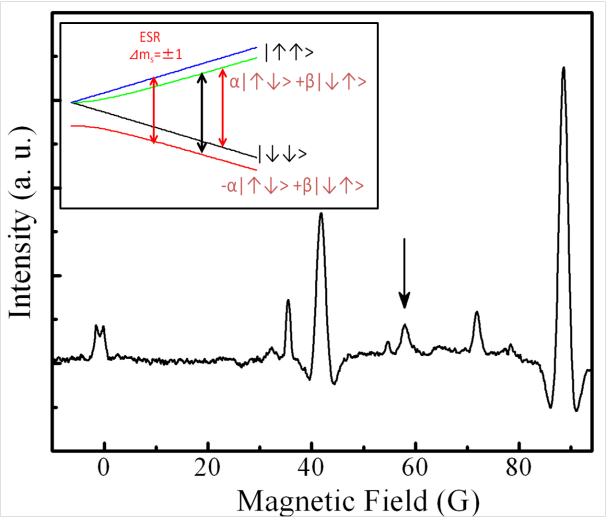

Figure 3.3: Phosphorus forbidden transition - EDMR spectra showing the forbidden transition in addition to the EPR allowed transitions of phohphorus. The signal was measured with an applied RF of 200 MHz. Such forbidden transition was not visible earlier with the [P] $\approx 10^{15}$ cm^{-3} in samples that were not irradiated with γ rays.

energy level at low magnetic field, where the hyperfine interaction between electron and nuclear spin of phosphorus is comparable with Zeeman term in spin Hamiltonian. The transition marked by black arrow in the inset of Fig. 3.3 is generally forbidden at high

magnetic field but the superposition of states formed at low field partially allows such transition.

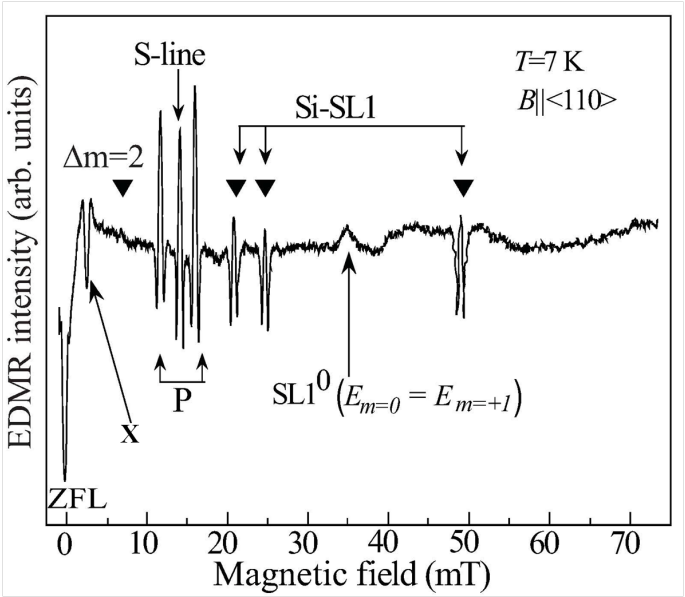

Figure 3.4: EDMR signals from phosphorus and SL1 centers - EDMR spectra detected in irradiated sample with the application of 400 MHz resonant frequency.

Figure 3.4 shows the complete EDMR spectra obtained with irradiation of 400 MHz resonance frequency. Positions of few of these lines (marked as Si-SL1) depend on the orientation of the crystal in magnetic field. Analysis of the line positions of the spectrum in Figure 3.4 shows that it arises from the excited spin S=1 state of oxygen+vacancy complex (A-center) which has been previously observed by traditional EPR [29] and EDMR spectroscopy [6, 7, 33]. The line positions calculated for orientation B$\|$ $\langle 110 \rangle$ using the spin Hamiltonian parameters determined in Ref. [10] are shown by triangles in Figure 3.4. The line at B=35mT corresponds to the anticrossing point of magnetic sublevels with spin projections m_s=+1 and m_s=0. The position of this line does not depend on the resonance frequency and could be observed even without resonance field. The negative line marked by X in Figure 3.4 is not identified. The mechanism of SDR responsible for Si-SL1 EDMR spectrum is well established [33] and caused by spin-selective transitions from excited triplet states of A-centers to ground singlet state which leads to non-equilibrium populations of triplet magnetic sublevels with spin projections m_s=+1,0,and -1,and to different signs of lines detected by traditional EPR technique [29]. The excitation of magnetic resonance transitions between magnetic sublevels in the excited triplet state increases the recombination rate and decreases the

photoconductivity of samples [33].

Thus, we have shown that the γ-irradiated samples contains predominantly two paramagnetics centers in the bulk, namely, phosphorus and SL1 centers. So, we believe that its the SDR process between the spin pairs of phosphorus and SL1 centers in the bulk which lead to the observed EDMR spectrum reported in the above section. These results motivates further studies using pulsed EDMR to read out the spin state of the bulk phosphorus electrons that have long coherence time in contrast to the surface phosphorus which suffers decoherence due to the magnetic noise from the paramagnetic Si/SiO_2 interface states [11, 12].

3.1.4 Conclusion

Electrically detected magnetic resonance(EDMR) of phosphorus donors, surface defects,and photoexcited Si-SL1 centers has been detected for relatively low resonance frequencies ($\leq$400 MHz) and magnetic fields($\leq$50 mT). The comparison of the phosphorus and surface EDMR lines intensities in the sample before and after γ-ray irradiation shows convincingly that the defects created through out the bulk region by the γ-ray are effective spin dependent recombination centers and they lead to strong enhancement of the phosphorus EDMR signal even at the concentration of radiation defects 10 times lower than concentration of phosphorus atoms. EDMR signal from the entangled states of phosphorous in silicon can also be observed in irradiated samples.The EDMR S-line with g$\approx$2.01 was identified as arising from surface recombination centers.The photoexcited triplet states of A-centers were also observed.

3.2 Electrically detected cross relaxation

Cross relaxation is the mechanism for the establishment of a common spin temperature in the spin reservoir by resonant energy exchange among the quantum system. In this section, we demonstrate electrical detection of cross relaxation processes (EDCR) in phosphorus doped γ -irradiated silicon, where the dipolar-coupled electron spins of phosphorus and oxygen-vacancy complex (Si-SL1 center) undergo spin flip-flop transitions at specific magnetic field values for which the Zeeman splitting of the two centers become equal. Such cross relaxation signals are observed as the change in the sample photoconductivity at theoretically predicted magnetic fields *without* application of resonance frequency. This makes EDCR a very simple and sensitive method for detecting paramagnetic centers in semiconductors.

3.2.1 Introduction

In the presence of external magnetic fields, the spin population among magnetic sublevels approaches the Boltzmann distribution in a time frame known as spin-lattice relaxation time (T_1) [13, 14] . When two different kinds of spins coexist in solid, they can achieve identical spin temperature through energy conserving flip-flop transitions, provided that their Zeeman energies are made nearly equal by tuning the magnetic field strength [15, 16, 17]. This phenomenon is known as cross relaxation and occurs if the exchange of energy between the two different spins is significantly faster than the exchange with the lattice, i.e. $\tau_{CR} < T_1$, where τ_{CR} is the cross relaxation time [18, 19]. In the past, optical detection of cross relaxation (ODCR) has been studied in solids, where the change in the luminescence intensity from one of two different dipolar coupled paramagnetic centers is monitored as their Zeeman splittings are brought into resonance by appropriate tuning of the magnetic field [20, 21]. However, the optical method can be used only if recombination through one or both the paramagnetic centers are radiative.

The present work reports electrical detection of cross relaxation (EDCR) between two different paramagnetic centers in silicon. So far, an electrical method for detecting magnetic resonance, widely known as electrically detected magnetic resonance (EDMR), has been demonstrated for a variety of condensed matter systems. EDMR detects change in photoconductivity via spin dependent recombination (SDR)[22, 34, 23, 24] or spin dependent scattering[25, 26] when target paramagnetic centers are brought into resonance with externally applied radio or microwave fields. The present work on the electrical method for detecting cross relaxation probes the change in photoconductivity when two different spin systems are brought into resonance by tuning the magnetic field. Unlike the case of electron paramagnetic resonance (EPR) and EDMR spectroscopy, EDCR does not require external irradiation to induce transitions between the magnetic sublevels because two different centers that are coupled by magnetic dipolar interactions undergo energy conserving flip-flop transitions. Therefore, EDCR measurement is as simple as monitoring photoconductivity under scanning magnetic field and applicable for detecting both radiative and non-radiative centers.

The present study focuses on the cross relaxation between electron spins of phosphorus and oxygen-vacancy centers (A-centers) in a γ-ray irradiated Czochralski (CZ)-grown, phosphorus (P)-doped silicon single crystal. A-centers are known to be the dominant defects created by irradiation of oxygen-rich CZ silicon [27, 28]. A-centers can be easily transformed by band-gap illumination into excited triplet states (electron spin S=1) that lead to well known Si-SL1 EPR spectra [29]. Thus, under illumina-

tion the sample contains predominantly two kinds of paramagnetic centers: phosphorus (S=1/2 and ^{31}P nuclear spin I=1/2) and Si-SL1 centers (S=1). Figure 3.5 shows the Zeeman levels of SL1 and phosphorus as a function of applied magnetic field. Cross relaxations are expected when Zeeman splittings of phosphorus and SL1 centers are made equal by tuning the magnetic field.

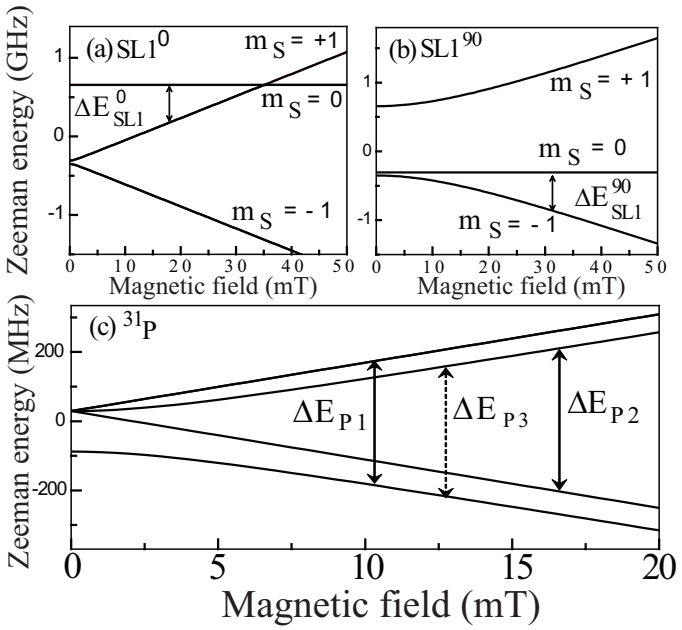

Figure 3.5: Zeeman energy - (a) Zeeman energy levels of SL1^0 center oriented along the direction of the magnetic field, (b) SL1^{90} center oriented at 90° to the applied magnetic field $B \| \langle 110 \rangle$, and (c) energy levels of phosphorus (^{31}P). ΔE^0_{SL1}, ΔE^{90}_{SL1} and $\Delta E_{P1,P2,P3}$ are the energy differences between the Zeeman levels (indicated by double-headed arrows) of SL1 centers and phosphorus, respectively. ΔE_{P3} is the forbidden transition which becomes observable only at low magnetic fields ($\leq$ 20 mT) due to the mixing of spin states [24].

The structure and spin Hamiltonian parameters of the triplet SL1 centers are well established [29]. SL1 center has orthorhombic symmetry represented by g and D-tensors. They orient along six different $\langle 110 \rangle$ crystal axes of the silicon lattice. When the magnetic field B is rotated in one of $\{110\}$ planes, the angle between magnetic field and one of the six groups of SL1 centers (represented by SL1^0 in Figure 3.5(a)) is varied from 0° ($B \| \langle 110 \rangle$) to 90° ($B \perp \langle 110 \rangle$). For the second group (represented by SL1^{90} in Figure 3.5(b)), the angle is always equal to 90°. The remaining four groups make intermediate angles with the magnetic field. Phosphorus in silicon, on the other hand, is a much simpler system of electron spin(S=1/2) coupled to a nuclear spin(I=1/2) via an isotropic hyperfine interaction $A/2\pi \approx 117.5$ MHz. Figure 3.5(c) shows the Zeeman

splitting between magnetic sublevels of phosphorus as a function of magnetic field [30].

The two centers interacting with each other through the long range dipole-dipole interaction which accounts for the flip-flop transition is given by[18]

$$\mathcal{H}_{\mathrm{DD}} = \frac{\gamma_P \gamma_{SL1} \hbar^2}{4r^3}(S_-^P S_+^{SL1})(1 - 3\cos^2\Theta), \tag{3.1}$$

where γ_P and γ_{SL1} are the gyro-magnetic ratios of phosphorus and SL1 centers, respectively, r is the distance between the two centers, $S_\pm = S_x \pm iS_y$ and Θ is the angle between the magnetic field direction and vector joining the two paramagnetic centers. The flip-flop transition probability ($W_{CR} = 1/\tau_{CR}$) is given by[18]

$$\begin{aligned} W_{\mathrm{CR}} &= \frac{2\pi}{\hbar^2} g_{CR}(\omega_{CR}) \\ &\quad \times \left|\langle m_p - 1, m_{SL1} + 1| \mathcal{H}_{\mathrm{DD}} |m_p, m_{SL1}\rangle\right|^2, \end{aligned} \tag{3.2}$$

where $\mathcal{H}_{\mathrm{DD}}$ is the dipolar Hamiltonian for flip-flop transition and $g_{CR}(\omega_{CR})$ is the overlap function for cross relaxation. For Gaussian line shapes, $g_{CR}(\omega_{CR})$ is given by

$$\begin{aligned} g_{CR}(\omega_{CR}) &= \frac{1}{2\pi(\Delta\omega_P^2 + \Delta\omega_{SL1}^2)^{1/2}} \\ &\quad \times \exp(-\frac{(\omega_P - \omega_{SL1})^2}{2(\Delta\omega_P^2 + \Delta\omega_{SL1}^2)^{1/2}}), \end{aligned} \tag{3.3}$$

where $\Delta\omega_P^2$ and $\Delta\omega_{SL1}^2$ are the second moments of line shapes of phosphorus and SL1, respectively. It can be seen from the above equations that the probability for the cross relaxation is maximal for the magnetic field at which the Zeeman frequencies ω_P and ω_{SL1} becomes equal, and its probability falls down significantly as the externally applied magnetic field shifts away from the equal point.

It is clear from the above discussions that the average distance between phosphorus and SL1 centers, i.e., the concentrations of the two centers, must be appropriate to achieve strong enough dipolar coupling for induction of cross relaxation. The observation of cross relaxation signals in this study is partially due to successful control of the concentration of phosphorus and SL1 centers in the sample.

3.2.2 Experimental

Rectangular shaped samples ($8 \times 4 \times 1$ mm^3) with the long edge along $\langle 110 \rangle$ crystal axis were cut from a Czochralski (CZ)-grown n-type single crystal silicon wafer having the phosphorus concentration $\sim 10^{15}$ cm^{-3}. Ohmic contacts for electrical measurements were made by ion implantation of arsenic (dose $\approx 10^{15}$ cm^{-2} at 25 keV) followed by

30s annealing at 950 °C and vacuum deposition of palladium and gold. After making ohmic contacts, samples were irradiated by γ-rays emitted from a ^{60}Co source at room temperature with the dose of $\sim 10^{15}$ cm^{-2} to produce $\sim 10^{13}$ cm^{-3} of A-centers throughout the sample volume. Prior to each measurement, the surface silicon dioxide was removed with dilute hydrofluoric acid (HF) solution to reduce the resonance due to surface defects.

EDCR measurements were performed at low temperatures ($T < 10$ K) in a helium bath cryostat having optical windows for illumination. A white light from a 100 W halogen lamp was focused on the sample through one of the optical windows of the cryostat. The change in sample photoconductivity under scanning magnetic field was measured using electrical contacts. A lock-in detector tuned to the second harmonic of magnetic field modulation at a frequency 5 KHz was employed to increase the signal to noise ratio. The signals were recorded as second derivatives of the magnetic field. The angular dependence of the cross relaxation line position was measured by rotating the sample about the $\langle 110 \rangle$ crystal axis.

The cross relaxation spectra were also detected with the same sample using the microwave SDR photoconductivity technique [31, 32, 33].

Here a X-band (9 GHz) EPR spectrometer was used and the change in photoconductivity of the sample was detected as the variation in the cavity Q factor since the change in the concentration of photo-excited carriers leads to change in the absorption of the microwave in the EPR cavity.

3.2.3 EDMR and EDCR spectra

Figure 3.6(a) shows the change in the photoconductivity (EDCR intensity) with sweeping magnetic field observed without application of external excitation field. The difference in signs of the signal is due to the phase of the lock-in amplifier used to optimize the signal to noise ratio.

Figure 3.6(b) shows the Zeeman energy splittings, ΔE_{SL1} and ΔE_P as defined in Fig.1, between the spin states of SL1 and phosphorus, respectively. It is apparent from Figure 4.6(a) and (b) that the EDCR signals appear as expected at magnetic fields where $\Delta E^0_{SL1} = \Delta E_{P1}, \Delta E_{P2}, \Delta E_{P3}$ and $\Delta E^{90}_{SL1} = \Delta E_{P2}$. Hereafter, these cross relaxation flip-flop transitions are referred to as $\Delta E^0_{SL1} \Leftrightarrow \Delta E_{P1}, \Delta E^0_{SL1} \Leftrightarrow \Delta E_{P2}, \Delta E^0_{SL1} \Leftrightarrow \Delta E_{P3}$ and $\Delta E^{90}_{SL1} \Leftrightarrow \Delta E_{P2}$ relaxations. The signal appearing at zero magnetic field, zero field line (ZFL), is due to the cross relaxation among degenerate levels. As reported by Bloembergen *et al* [18]. the cross relaxation can occur even within

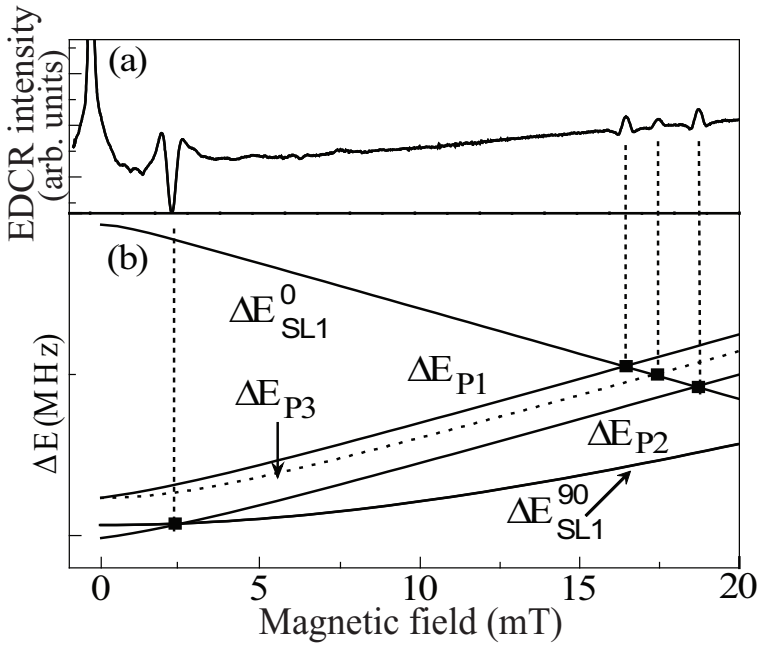

Figure 3.6: EDCR signal and crossing of Zeeman energy - (a) An EDCR spectrum showing the change in photoconductivity (EDCR intensity) with scanning magnetic field $B \| \langle 110 \rangle$, T= 7 K with no resonance frequency. (b) Calculation showing the magnetic field dependence of the $\Delta E's$ as defined in Fig.3.5. Solid squares (■) in (b) show the crossing points between $\Delta E's$ of SL1 center and phosphorus for $B \| \langle 110 \rangle$, where the occurrence of cross relaxations is expected.

a single paramagnetic center having three or more magnetic sublevels. Both phosphorus and SL1 centers have degenerate energy levels at zero magnetic field which contribute to the zero field signal.

The electrically detected magnetic resonance (EDMR) spectroscopy was used to validate the presence of phosphorus and SL1 centers in our sample. Figure 3.7 shows the EDMR spectrum from phosphorus doped γ-irradiated silicon at 7 K with externally applied RF field of 400 MHz. The EDMR spectrum shows the resolved ^{31}P hyperfine doublet separated by 4.2 mT and fine structures of the SL1 centers as expected [34, 33, 35]. These EDMR signals confirms the presence of phosphorus and SL1 centers in the sample.The signal marked SL1 $^0(E_{m=0} = E_{m=+1})$ in Figure 3.7 arises at the anticrocssing point of $m_s = 0$ and $m_s = +1$ states in Figure 3.5(a) and can be observed even without application of the resonance field. This signal is due to mutual flip-flops between the $m_s = 0$ and $m_s = +1$ states of SL1 centers that are oriented along the externally applied magnetic field.

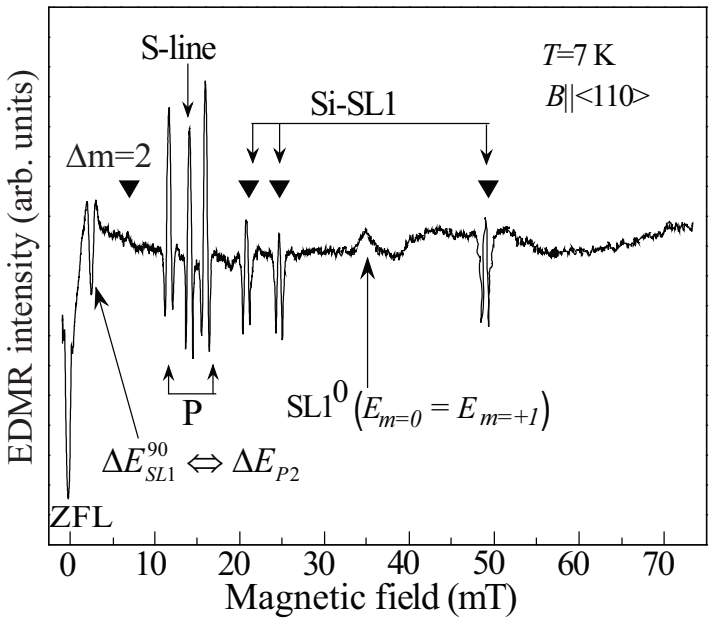

Figure 3.7: EDMR spectrum from phosphorus doped γ-irradiated silicon - An EDMR spectrum showing spin dependent recombination signals in phosphorus doped γ-irradiated silicon recorded with application of 400 MHz resonance field, $B \| \langle 110 \rangle$, and T =7 K. Along with phosphorus hyperfine lines (P), signals from SL1 centers (Si-SL1) and surface centers(S-line) were observed. Solid triangles indicate calculated line positions of SL1 signals using the parameters reported in Ref.18. The cross relaxation signal marked $SL1^0(E_{m=0} = E_{m=+1})$, is independent of applied resonance frequency and appears at the anticrossing point of m_s=0 and m_s=+1 states of $SL1^0$ and is observed even when the RF is turned off.

Figure 3.8 shows EDMR spectra recorded with three different RF field. The line positions of the cross relaxation signals (dotted lines) are independent of the irradiated frequency as expected, while positions of EDMR signals shift along with the resonance frequency. These results further substantiate our understanding of cross relaxation processes, which are independent of the applied RF field.

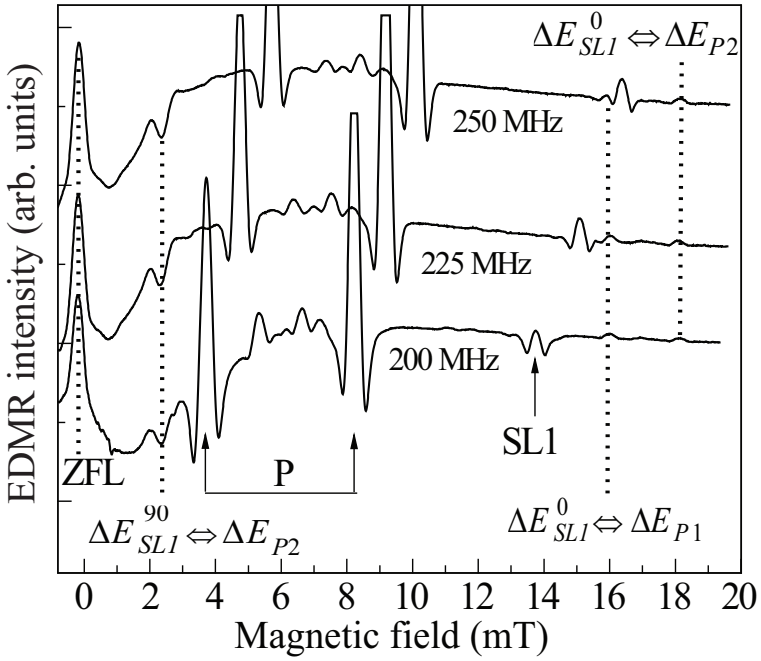

Figure 3.8: Effect of oscillating field on EDCR lines - EDMR spectrum with three different resonance frequency for $B \| \langle 110 \rangle$ and T=7 K. Positions of phosphorus (P) and SL1 EDMR signals (marked by solid arrows) shift with the frequency, while the positions of EDCR signals (marked by dotted lines) are independent of the frequency.

3.2.4 Angular dependence of EDCR line positions

In contrast to isotropic EPR and EDMR spectra of phosphorus, the SL1 centers exhibit strong anisotropy in the line positions with respect to the direction of applied magnetic field [29, 33]. Thus, the line positions of EDCR signals arising from phosphorus and SL1 centers should also be anisotropic.

Figure 3.9 shows the experimentally observed EDCR line positions when the sample is rotated about the $\langle 110 \rangle$ crystal axis. The angular dependence of $\Delta E^{90}_{SL1} \Leftrightarrow \Delta E_{P2}$ is very weak as compared to the lines labeled as I, II, III and IV that show very strong anisotropy. Our EDCR experimental setup is currently limited to rotation of the sample up to 45°. Thus, in order to obtain the complete angular dependence in the 0° ($B \| \langle 110 \rangle$) to 90° ($B \| \langle 100 \rangle$) range, the cross relaxation line positions were obtained by the contact free microwave photoconductivity technique using the X-band EPR spectrometer. Experimental results are shown in Figure 3.10.

The angular dependence of cross relaxation line positions observed by EDCR (Figure 3.9) and microwave photoconductivity (Figure 3.10(b)) are essentially the same.

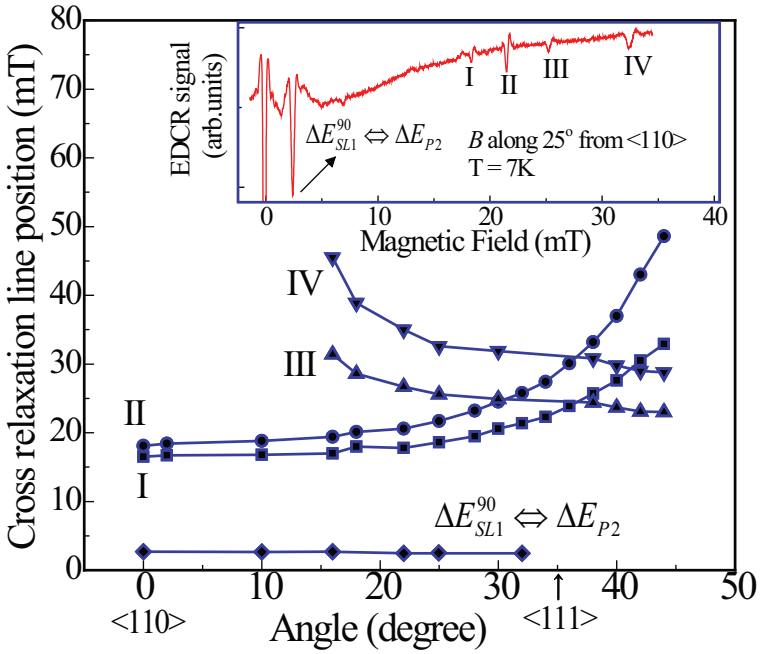

Figure 3.9: Angular dependence of EDCR lines - Angular dependence for the line position of EDCR signal from phosphorus doped γ-irradiated silicon. Inset shows the EDCR spectrum when the external magnetic field is applied along 25° from $\langle 110 \rangle$.

Moreover, the experimentally observed cross relaxation line positions show excellent agreement with theoretically calculated line positions represented by solid curves in Figure 3.10(b). Calculations were performed for each of six possible orientations of SL1 centers in a silicon crystal. $\Delta E^{90}_{SL1} \Leftrightarrow \Delta E_{P2}$ line has very weak angular dependence and attributed to cross relaxation between electron spins of phosphorus and SL1 centers which are oriented perpendicular to the magnetic field throughout the rotation around $\langle 110 \rangle$ axis. Lines I and II originate from cross relaxation between phosphorus and SL1 centers oriented in $\{110\}$ plane. Remaining four orientations of SL1 centers are responsible for lines III, IV, V and VI.

The excellent correlation between the experimental and theoretically calculated angular dependences confirms that the spin flip-flop process between phosphorus and spin triplet SL1 centers is responsible for EDCR signals detected in this study.

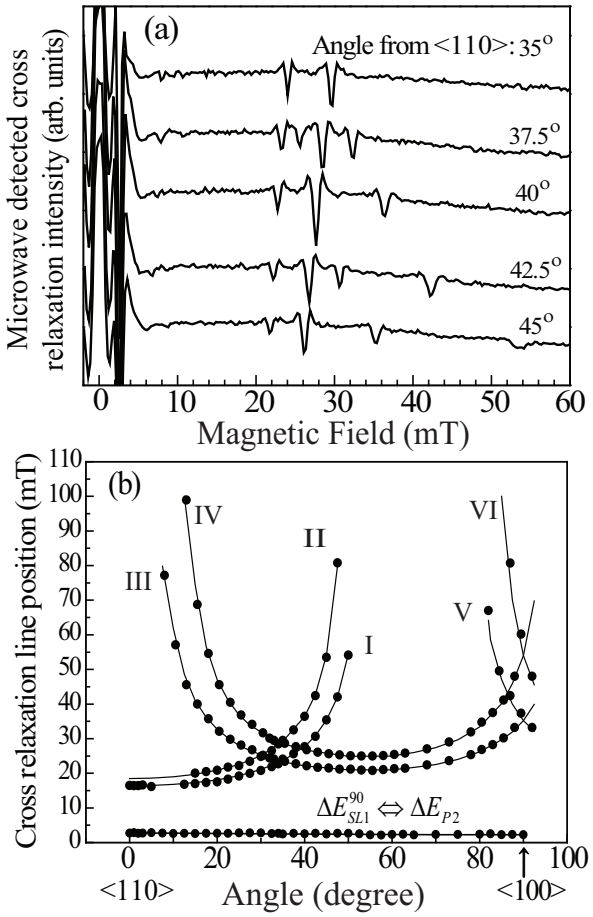

Figure 3.10: Complete angular dependence measured using microwave photoconductivity technique - (a) Cross relaxation signals detected by the microwave photoconductivity technique and (b) angular dependences of their positions revealed by the microwave-photoconductivity technique. Dots (•) represents the experimentally obtained line positions of cross relaxation signals and curves represent the calculated positions of Zeeman energy crossing points between phosphorus and SL1 centers. Signals marked as I,II,III,IV,V and VI originates from SL1 centers having different orientations in the crystal.

3.2.5 Model for the observed photoconductivity change under cross relaxation

To explain the change in photoconductivity by cross relaxation, we construct a simple model for spin dependent recombination of photo excited carriers through the excited spin S=1 states of A-centers coupled with paramagnetic phosphorus (P) atoms by long-range dipolar interaction. P and SL1 centers separated by a distance of r can exchange

energy by the spin flip-flop process, when their Zeeman splittings are made nearly equal by tuning the magnetic field strength. The energy ΔE_P released by the electron bound to phosphorus through relaxation from m_S=+1/2 to m_S=−1/2 is absorbed by the SL1 center to induce transition from m_S=0 to m_S=+1.These flip-flop transitions change the populations among the magnetic sublevels of SL1 centers. The steady state population n_+, n_0 and n_- for spin projections m_S=+1, m_S=0 and m_S=−1, respectively, of SL1 centers can be found from the following rate equations,

$$\frac{dn_+}{dt} = G_T - k_+n_+ - (n_+ - n_0)(W + W_{CR}), \tag{3.4a}$$

$$\frac{dn_0}{dt} = G_T - k_0n_0 - (2n_0 - n_+ - n_-)W - (n_0 - n_+)W_{CR}, \tag{3.4b}$$

$$\frac{dn_-}{dt} = G_T - k_-n_- - (n_- - n_0)(W + W_{CR}). \tag{3.4c}$$

For steady state solution $\frac{dn_+}{dt}$=$\frac{dn_0}{dt}$=$\frac{dn_-}{dt}$=0. Here G_T is the generation rate of triplet states under illumination, which is same for m_S=+1, m_S=0 and m_S=−1 states. k_+, k_0, and k_- are the transition probabilities from m_S=+1, 0 and −1 to the ground singlet state, respectively. In zero order approximation these transitions are forbidden, but taking into account the spin-orbit interaction, the probabilities k_+, k_0 and k_- are non-zero and $k_+ = k_- \neq k_0$.[36] W_{CR} is the probability of cross relaxation caused by other paramagnetic centers when the Zeeman splitting between these centers coincide with the splitting between m_S=+1 and m_S=0 states. W is the spin lattice relaxation probability.

The generation and recombination of photoexcited carriers can be described by the simple rate equation,

$$\frac{dn_e}{dt} = G - R_An_e(N - N_T) - Rn_e, \tag{3.5}$$

where G is the generation rate of electrons by light, N is the concentration of A-centers and N_T is the concentration of A-centers in the excited triplet state. The second term describes the rate of formation of excited triplet states by electron recombination through A-centers [37]. The last term in Eq.(3.5) corresponds to the rate of electron recombination R through other defects in the sample. Using Eqs. (3.4) and (3.5), the change in photoconductivity under cross relaxation can be calculated as the difference between the steady state populations of photo-excited electrons for $W_{CR} \neq 0$ and W_{CR} = 0, i.e., Δn_e=$n_e(W_{CR})$-$n_e(0)$.

The important parameters for detection of EDCR signals are the ratio of the cross relaxation rate to spin lattice relaxation rate, W_{CR}/W, and the ratio of the spin lattice relaxation time ($T_1 = 1/W$) to the life time (τ_T) of the excited triplet states. Figures

3.11(a) and (b) show the dependence of $\Delta n_e/n_e(0)$ on the ratio W_{CR}/W for different values of T_1/τ_T and on the ratio T_1/τ_T at fixed value of W_{CR}/W=10. The calculations were performed for R_+=R_-=$10R_0$. These results have very weak dependence on the values of the parameters N, G, R_A, and R.

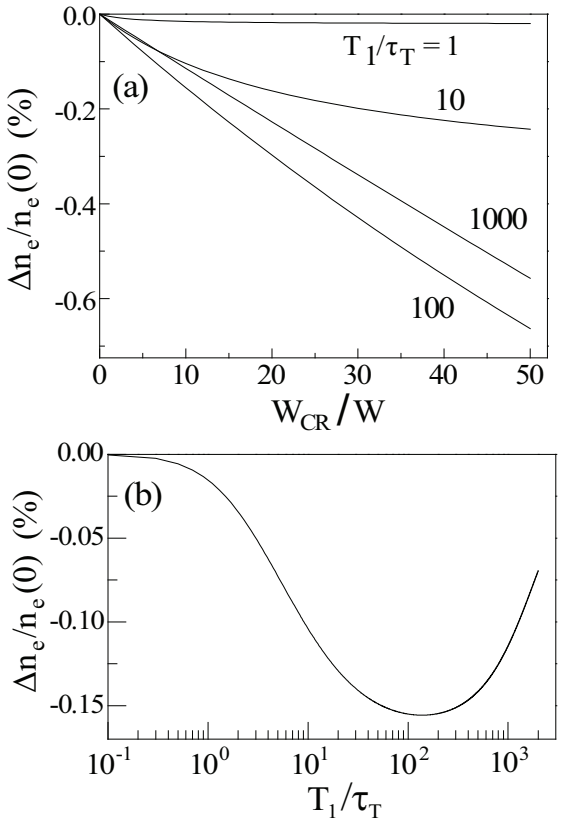

Figure 3.11: Enhancement of recombination due to cross relaxation - (a) The relative change of $\Delta n_e/n_e(0)$ as a function of W_{CR}/W for different values of T_1/τ_T and (b) $\Delta n_e/n_e(0)$ as a function of T_1/τ_T for $W_{CR}/W = 10$.

Figure 3.11 shows that the change in photoconductivity due to cross relaxation (which is proportional to Δn_e) is negative corresponding to the increase in the recombination rate at the onset of cross relaxation process. The absolute value of Δn_e increases with the increase of the cross relaxation rate W_{CR} at fixed W. As follows from Figure 3.11(b), the EDCR signals can be observed for a wide range of T_1/τ_T ratio. However, for the observation of cross relaxation signals following condition should be satisfied,

$$\frac{1}{\tau_{CR}} > \frac{1}{\tau_T} > \frac{1}{T_1}, \tag{3.6}$$

where τ_{CR} is the cross relaxation time, τ_T is the decay lifetime of the SL1 center and T_1 is the spin relaxation time of the SL1 center. The first inequality is important for the occurrence of the cross relaxation before the SL1 center decays. The second inequality defines the criteria for the existence of nonequilibrium population distribution among the magnetic sublevels of SL1 centers. For these triplet centers, the spin lattice relaxation time $T_1 \sim 10$ s, is significantly longer than their life time $\sim 10^{-3}$ s.[38], thus the last inequality in Eq.(3.6) is satisfied. The cross relaxation time (τ_{CR}), limited by the lifetime of SL1 centers should be $\leq 10^{-3}$ s. Assuming that the EPR line shape is Gaussian, it can be estimated using Eqs.(3.1)$\sim$(3.3) that a phosphorus and SL1 pair separated by $r \leq 20$ nm has cross relaxation time $\tau_{CR} \leq 10^{-3}$ s. Irradiation of the sample by γ-rays emitted from a ^{60}Co source at room temperature with the dose of $\sim 10^{15}$ cm^{-2} produces $\sim 10^{13}$ cm^{-3} of A-centers throughout the sample volume. However, the above band gap illumination intensity employed in the experiment limits the concentration of triplet excited state to $\sim 10^{11}$ cm^{-3}, i.e., $\sim 10^9$ SL1 centers in the bulk of the sample. The average separation between phosphorus atoms for the concentration of 10^{15} cm^{-3} is ~ 100 nm. If we assume one phosphorus atom interacting with one SL1 center then there are $\sim 10^9$ phosphorus-SL1 pairs with the separation r between the centers distributed randomly between $0-50$ nm (half the distance between phosphorus atom). The probability that SL1 center will be found in the sphere of radius r from the phosphorus atom is clearly $r^3/(50)^3$. Thus, we estimate that $\sim 10^8$ pairs of phosphorus-SL1 centers with the separation distributed within the sphere of radius ≤ 20 nm, contributes to the EDCR signal observed in this study.

3.2.6 Conclusion

Electrical detection of cross relaxation between electron spins of phosphorus and SL1-centers in silicon has been demonstrated experimentally. The flip-flop transitions led to change in the sample photoconductivity at theoretically expected externally applied magnetic fields. The angular dependence of the cross relaxation peak positions also agrees well with calculated values reflecting the symmetry of SL1 centers. The change in the photoconductivity originates from the difference in the lifetimes of magnetic sublevels of triplet states of SL1 centers that changes the electron-hole recombination time at occurrence of cross relaxation. The experimental observation of EDCR signals require the cross relaxation rate to be higher than the decay rate of triplet centers which in turn must exceed the spin lattice relaxation rate.These conditions are satisfied for SL1 centers situated within the sphere of radius $r \leq 20$ nm from each phosphorus atom. The electrical detection of cross relaxation is a very simple and sensitive technique to investigate variety of defects in semiconductors.

Bibliography

[1] J. Shmidt and I. Solomon, Compt. Rend. **263**, 169 (1966). (Cited on page 35.)

[2] A. Honig, Phys. Rev. Lett. **17**, 186 (1966). (Cited on page 35.)

[3] D. D. Thorntont and A.Honig, Phys. Rev. Lett. **30**, 909 (1973). (Cited on page 35.)

[4] D. J. Lepine, Phys. Rev. B. **6**, 436 (1973). (Cited on page 35.)

[5] D. Kaplan, I. Solomon and N. F. Mott, J. Phys. Lett. **39**, L5l (1978). (Cited on page 35.)

[6] L. S. Vlasenko and V. A. Khramtsov, Sov. Phys. Semicond. **20**, 688 (1986). (Cited on pages 35 and 39.)

[7] B. Stich, S. Greulich-Weber and J. M. Spaeth, J. Appl. Phys. **77**, 1546 (1994). (Cited on pages 35 and 39.)

[8] A. R. Stegner, C. Boehme, H. Huebl, M. Stutzmann, K. Lips and M. S. Brandt, Nat. Phys. **2**, 835 (2006). (Cited on pages 36 and 42.)

[9] K. L. Brower, Phys. Rev. B. **4**, 1968 (1971). (Cited on pages 39, 42, 43 and 48.)

[10] L. S. Vlasenko, M. P. Vlasenko, V. N. Lomasov and V.A.Khramtsov, Sov. Phys. JETP **64**, 612 (1986). (Cited on pages 39, 40, 45, 46 and 48.)

[11] T. Schenkel, J. A. Liddle, A. Persaud, A. M. Tyryshkin, S. A. Lyon, R. de Sousa, K. B. Whaley, J. Bokor, J. Shangkuan and I. Chakarov, Appl. Phys. Lett., **88**, 112101 (2006). (Cited on page 40.)

[12] H. Huebl, F. Hoehne, B. Grolik, A. R. Stegner, M. Stutzmann, and M. S. Brandt, Phys. Rev. Lett., **100**, 177602 (2010). (Cited on page 40.)

[13] F. Bloch, Phys. Rev. **70**, 1 (1945). (Cited on page 42.)

[14] H. B. G. Casimir and F. K. DuPre, Physica **5**, 507 (1938). (Cited on page 42.)

[15] G. Feher and H. E. D. Scovil, Phys. Rev. **105**, 760 (1956). (Cited on page 42.)

[16] A. Abragam and W. G. Proctor, Phys. Rev. **109**, 1441 (1958). (Cited on page 42.)

[17] Robert T. Schumacher , Phys. Rev. **112**, 837 (1958). (Cited on page 42.)

[18] N. Bloembergen, S. Shapiro, P. S. Pershan and J. O. Artman, Phys. Rev. **114**, 445 (1959). (Cited on pages 42, 44 and 45.)

[19] P. S. Pershan, Phys. Rev. **117**, 109 (1960). (Cited on page 42.)

[20] K. M. Lee and G. D. Watkins, Phys. Rev .B **26**, 26 (1982). (Cited on page 42.)

[21] E. Van Ooat and M. Glasbeck, Phys. Rev. B. **40**, 6509 (1989). (Cited on page 42.)

[22] D. Kaplan, I. Solomon and N. F. Mott, J. Phys. Lett. **39**, L51 (1978). (Cited on page 42.)

[23] A. R. Stegnar, C. Boehme, H. Huebl, M. Stutzman, K. Lips, and M. S. Brandt, Nat. Phys. **2**, 835 (2006). (Cited on pages 36 and 42.)

[24] H. Morishita, L. S. Vlasenko, H. Tanaka, K. Semba, K. Sawano, Y. Shiraki, M. Eto and K. M. Itoh, Phys. Rev. B **80**, 205206 (2009). (Cited on pages 42 and 43.)

[25] A. Honig, Phys. Rev. Lett. **17**, 186 (1966). (Cited on page 42.)

[26] D. D. Thorntont and A. Honig, Phys. Rev. Lett. **30**, 909 (1973). (Cited on page 42.)

[27] G. D. Watkins, J. W. Corbett and R. M. Walker, J. Appl. Phys **30**, 1198 (1959). (Cited on page 42.)

[28] J. W. Corbett, G. D. Watkins, R. M. Chrenko and R. S. McDonald, Phys. Rev. **121**, 1015 (1961). (Cited on page 42.)

[29] K. L. Brower, Phys. Rev. B **4**, 1968 (1971). (Cited on pages 39, 42, 43 and 48.)

[30] G. Feher and E. A. Gere, Phys. Rev. **114**, 1245 (1959). (Cited on page 44.)

[31] L. S. Vlasenko, Yu. V. Martynov, T. Gregorkiewicz, and C. A. J. Ammerlaan, Phys. Rev. B **52**, 1144 (1995). (Cited on page 45.)

[32] L. S. Vlasenko, V. A. Khramtsov, Sov. Phys. Semicond. **20**, 688 (1986). (Cited on page 45.)

[33] L.S. Vlasenko, M.P. Vlasenko, V.N. Lomasov, V.A.Khramtsov, Sov. Phys. JETP, **91**, 1037 (1986). (Cited on pages 39, 40, 45, 46 and 48.)

[34] B. Stich, S. Greulich-Weber, and J.-M. Spaeth, J. Appl. Phys. **77**, 1546 (1995). (Cited on pages 42 and 46.)

[35] W.Akhtar, H. Morishita, L. S. Vlasenko, D. S. Poloskin and K.M. Itoh, Physica B, **404** , 4583 (2009). (Cited on page 46.)

[36] S. P. McGlynn, T. Azumi, M. Kinosita, Molecular spectroscopy of the triplet state, Prentice-Hall, Englewood Cliffs, NJ (1969). (Cited on page 51.)

[37] A^{0*}-centers (SL1-centers) are created by the capture of photoexcited electrons (e) and holes (h) by (A^0),(A^+) and(A^-) centers according to reaction $A^0 + e \rightarrow A^- + h \rightarrow A^{0*} \overset{R_+,R_0,R_-}{\longrightarrow} A^0$ or $A^0 + h \rightarrow A^+ + e \rightarrow A^{0*} \overset{R_+,R_0,R_-}{\longrightarrow} A^0$,where the transitions $A^{0*} \longrightarrow A^0$ are spin dependent. Under illumination, a part of A-centers ($N_T = n_+ + n_0 + n_-$) is in the excited triplet state (A^{0*}). And the remaining,$N_0 = N - N_T$, are in the positive (A^+), negative (A^-) and in the neutral singlet (A^0) charge states. Here, N is the total concentration of A-centers in the sample. (Cited on page 51.)

[38] L. S. Vlasenko, I. M. Zaritskii, A. A. Konchits, B. D. Shanina, Sov. Phys. Solid State, **26**, 66 (1984). (Cited on page 53.)

Chapter 4

pEPR study of SL1 center

The metastable triplet states of oxygen-vacancy centers has been previously studied by EPR spectroscopy to understand the atomic constituents of the defect, however very little is known about their dynamical properties and the interaction of the triplets with the nuclear spins in the lattice. The strong hyperfine coupling of the triplets with the nearest neighbor ^{29}Si nuclear spin has been resolved in the cw-EPR spectrum, but we can not neglect the possibility of weak hyperfine coupling with the distant nuclear spins which goes unresolved in cw-EPR. In this chapter, we present the pulsed EPR study of these oxygen-vacancy centers in the presence of magnetic field. We found that the populating rates of the triplet sublevels are almost equal however, the decay to the ground singlet state is different for the sublevels. Moreover, the decay rates depends upon the direction of the externally applied magnetic field. Further, we have utilized electron spin echo envelop modulation (ESEEM) spectroscopy to resolve the weak hyperfine interaction with distant nuclear spins in the lattice and this results would help in understanding the extent of triplet state wave-function in the lattice. For the purpose of these experiments we have used electron beam irradiated (energy $\approx$ 1 MeV, dose $\approx 10^{18}$ cm^{-2}) Cz-grown single crystal natural silicon wafer. Pulsed EPR measurements were carried out at X-band (9.72 GHz) on a Bruker Elexsys580 spectrometer equipped with a helium-flow cryostat. Photoexcitation of the SL1 was achieved using a 1064 nm pulsed Nd:YAG laser (pulse width $\sim$ 7 ns, 1 mJ/pulse) with a 10 Hz repetition rate.

4.1 Lifetime of photoexcited triplets:SL1 centers

Figure 4.1(a) illustrates the SL1 center in silicon under two representative orientations of the static magnetic field B_0. Under one orientation, termed $SL1^0$, the magnetic field lies in the plane, marked (110), comprising the oxygen atom and two vacancy-trapping silicon atoms (i and j lattice sites). An alternative orientation ($SL1^{90}$) has the magnetic field in an orthogonal plane $(1\bar{1}0)$ with respect to the same center. Both planes are equivalent by symmetry for the crystal as a whole, so both orientations are visible in the EPR spectrum.

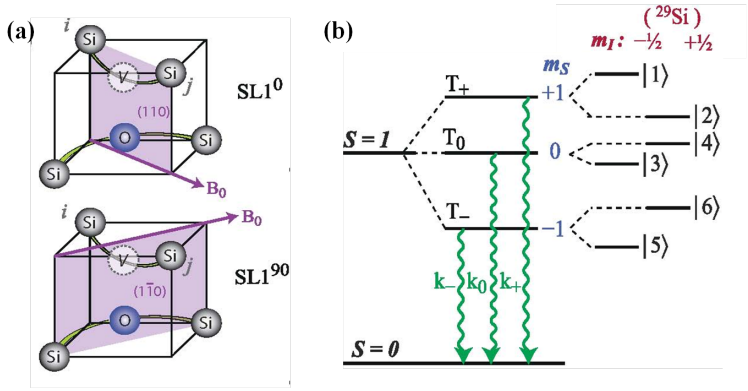

Figure 4.1: SL1 orientation and decay model - (a) Structures of the oxygen-vacancy centre in silicon, illustrating the $SL1^0$ and $SL1^{90}$ orientations with respect to the externally applied magnetic field B_0. (b) The SL1 triplet ($S = 1$) state is Zeeman split by B_0 into levels T_+, T_0, and T_-. These states decay with different rates (k_+, k_0, and k_-, respectively) to the ground singlet ($S = 0$) state.

Figure 4.1(b) shows the triplet energy sub-levels in the presence of a static magnetic field (T_+, T_0, and T_-), each of which decays with a characteristic rate to the ground singlet state [2, 3]. The hyperfine coupling with one of the two nearest-neighbor ^{29}Si nuclear spins (occupying i or j lattice site) further split the $T_{\pm1}$ sub-levels, while the T_0 state ($m_s = 0$) has no first-order hyperfine interaction, thus the nuclear spin splitting in this sub-level is close to the Zeeman energy of ^{29}Si. The EPR spectrum obtained by monitoring the electron spin echo intensity as a function of magnetic field at 12 K with $B_0 \| \langle 110 \rangle$ is shown in Figure 4.2, labeled with electronic transitions identified by previous cw-EPR studies [1].

The satellite peaks accompanying each main peak are due to the hyperfine interaction with the ^{29}Si nuclear spins situated at i or j lattice sites. The phase difference of the spin echo (i.e. dips or peaks) is indicative of the non-equilibrium polarization within

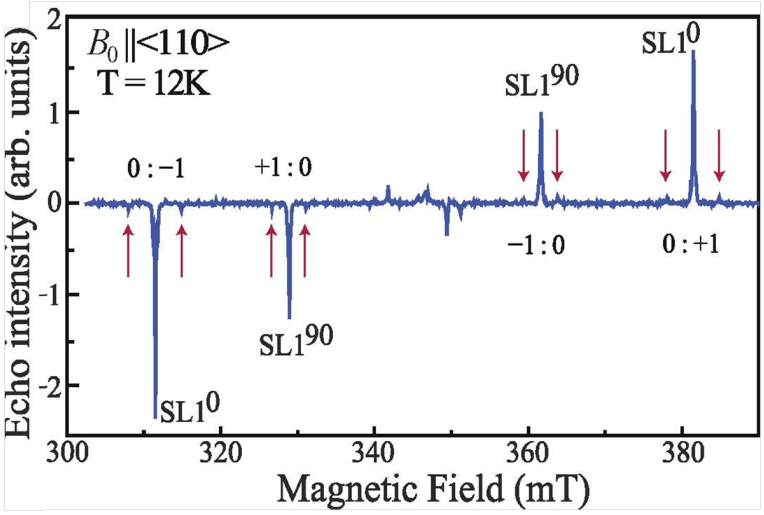

Figure 4.2: EPR spectruml - Electron spin echo-detected EPR spectrum of the SL1 center at 12 K with $B_0 \| \langle 110 \rangle$. The satellite peaks (red arrows) arise from hyperfine coupling to ^{29}Si sitting at i or j site (Figure 4.1) .

the electron spin triplet.

To investigate the origin of this non-equilibrium polarization, we studied the decay kinetics of the triplet by measuring the electron spin echo at a variable time T after the optical excitation ($h\nu - T - \pi/2 - \tau - \pi - \tau - echo$), as shown in Figure 4.3.

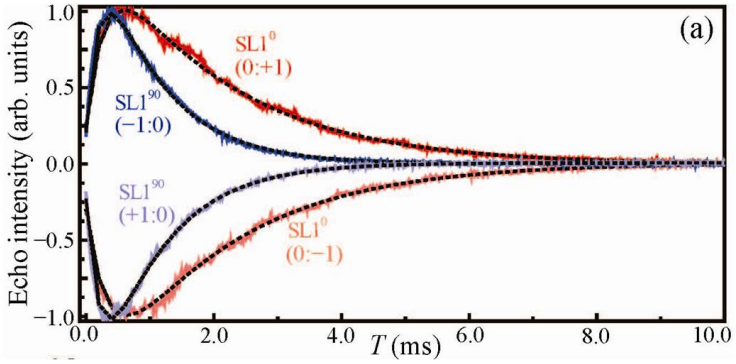

Figure 4.3: Decay kinetics - Decay traces obtained by the flash delay ($h\nu$-T-$\pi/2$-τ-π-τ-$echo$) pulse sequence, used to extract the triplet decay rates shown in Table 4.1. Black dotted line is the bi-exponential fit to the experimental data.

The zero echo intensity at $T = 0$ indicates equal initial filling of the three triplet sub-levels upon creation of the triplet. The echo intensity proceeds to grow as T is increased. This can be attributed to a difference in the decay rates of the triplet sub-levels to the ground state, creating a build-up in spin polarisation (positive or negative)

across the EPR transition being measured.

Based on the simple decay model shown in Fig. 1(b), the decay kinetics of the excited triplet state of A-centers (SL1 centers) can be described by following rate equations,

$$\begin{aligned} \frac{dn_+}{dt} &= -n_+k_+, \\ \frac{dn_0}{dt} &= -n_0k_0, \\ \frac{dn_-}{dt} &= -n_-k_-, \end{aligned} \tag{4.1}$$

where n_+,n_0 and n_- represents the population in the states with the spin projections m=+1, 0 and -1, respectively. Our model assumes that there is negligible spin-lattice relaxation within the triplet sub-levels, and this is consistent with lack of temperature dependence we observe in the relaxation dynamics below 20 K.

The echo intensity is directly proportional to the population difference between a given pair of sub-levels (echo intensity $\propto (n_+(t) - n_0(t))$) which follows a biexponential behavior where the two time constants represent the lifetimes of the two sub-levels involved in the EPR transition. The time constants obtained from biexponential fitting to the FD curves are given in Table 4.1 — the assignment of rates to particular energy levels is enabled by electron nuclear double resonance experiments described further below. As the transition from the triplet to the ground singlet is determined by the amount of singlet admixture to the triplet via spin-orbit coupling, the lifetimes are expected to depend on the defect orientation with respect to the magnetic field. The composition of tripet levels $T_{+,0,-}$ can be expressed in terms of the zero-field eigenstates ($T_{X,Y,Z}$), and similarly the observed decay rates from these levels can be traced back to a corresponding mixture of zero-field decay rates ($k_{X,Y,Z}$), as shown in Table 4.1.

It should be noted that the sum of the decay rates in the presence of magnetic field and in the zero-field limit should be same. Thus,

$$k_X + k_Y + k_Z = k_{+1} + k_0 + k_{-1} \tag{4.2}$$

The transition rates k_m from the triplet $T_m(m_s = 0, \pm 1)$ is proportional to the square of the matrix element of the spin-orbit coupling operator $\mathcal{H}_{SO}$:

$$k_m \propto |\langle S | \mathcal{H}_{SO} | T_M \rangle|^2 \tag{4.3}$$

Table 4.1: Lifetime of triplet sub-levels, for two orientations of SL1 centers, obtained from fitting to the flash delay curve.

EPR transition	Lifetime
$0 \rightarrow +1$, $SL1^0$	$(1/k_0)^0$= 2000(4) μs, $(1/k_{+1})^0$= 280(2) μs
$0 \rightarrow -1$, $SL1^0$	$(1/k_0)^0$= 1970(4) μs, $(1/k_{-1})^0$= 330(2) μs
$-1 \rightarrow 0$, $SL1^{90}$	$(1/k_{-1})^{90}$= 960(2) μs, $(1/k_0)^{90}$= 200(1) μs
$+1 \rightarrow 0$, $SL1^{90}$	$(1/k_{+1})^{90}$= 987(2) μs, $(1/k_0)^{90}$= 205(1) μs
$k_X = 1.6(3)$ ms^{-1}, $k_Y = 4.93(6)$ ms^{-1}, $k_Z = 0.50(4)$ ms^{-1}	

And it can be seen from above equation that $k_+ = k_- \neq k_0$, e.i. the decay rate from the T_+ and T_- is equal but differs from T_0. As, $k_+ = k_-$ and using Eqn. 4.2 we have:

$$k_+ = k_- = (k_X + k_Y)/2, for SL1^0, \tag{4.4}$$

and

$$k_+ = k_- = (k_X + k_Z)/2, for SL1^{90}, \tag{4.5}$$

Figure 4.4 is the schematic of the SL1 centers in the presence of magnetic field B_0. X, Y and Z represent the principle axis of the defect.

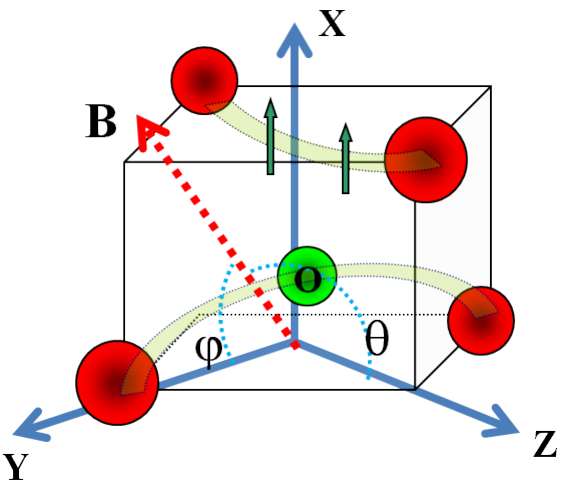

Figure 4.4: Principle axis of the defect - Schematic showing the SL1 center in presence of magnetic field B_0. X, Y and Z represents the principle axis of the defect.

The decay rate in the presence of magnetic field can be represented in the form of

zero-field decay rates using the coordinate transformation from laboratory frame to the principle axis of the defect, thus giving

$$k_0 = k_X(\sin^2\theta\cos^2\phi) + k_Y(\sin^2\theta\sin^2\phi) + k_Z\cos^2\theta, \tag{4.6}$$

For, $SL1^0$ orientation, $\theta = 0$, thus $(k_0)_{SL1^0} = k_Z$. For, $SL1^{90}$ orientation $\theta = 90, \phi = 0$, thus $(k_0)_{SL1^{90}} = k_Y$. Using Eqn. 4.4, 4.5 and 4.6, we can get the value of k_X, k_Y and k_Z to be $1.6 \times 10^3, 4.93 \times 10^3$ and $0.5 \times 10^3 s^{-1}$, respectively.These values are in good agreement with times measured using zero-field EPR [4].

Neverthless, in order to probe the dynamics in more detail, we can introduce an additional inversion π pulse to the sequence: ($h\nu$-T_X-π-T_Y-$\pi/2$-τ-π-τ-*echo*). Figure 4.5(a) shows the 2D plot of the echo intensity for this sequence, as both T_X (the delay after the laser pulse) and T_Y (the delay after the inversion pulse) are varied. The simulation of this experiment (Figure 4.5(b)), based on the model described above, is in good agreement with the observed behavior, supporting our assumption that spin-lattice relaxation can be neglected.

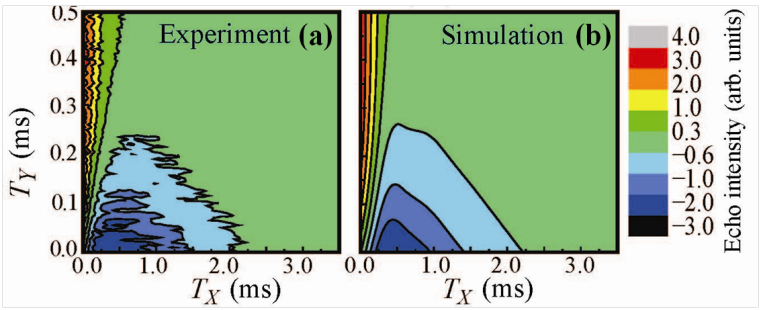

Figure 4.5: Decay kinetics - (a) Experimental and (b) simulated 2D plots of the decay characteristics observed with the pulse sequence $h\nu$-T_X-π-T_Y-$\pi/2$-τ-π-τ-*echo*.

Based on the observed decay rates, we can extract both the polarization buildup (Figure 4.6(a)) and the triplet population (Figure 4.6(b)) for the two SL1 orientations ($SL1^0$ and $SL1^{90}$) as a function of time T after the laser pulse. The maximum electron polarization reaches $> 99\%$ after about 1.5 ms following the laser pulse. Using such well initialized spin system and its strong coupling with the nearest neaighbor ^{29}Si nuclear spin, we will demonstrate ^{29}Si quantum memory in Chapter 5.

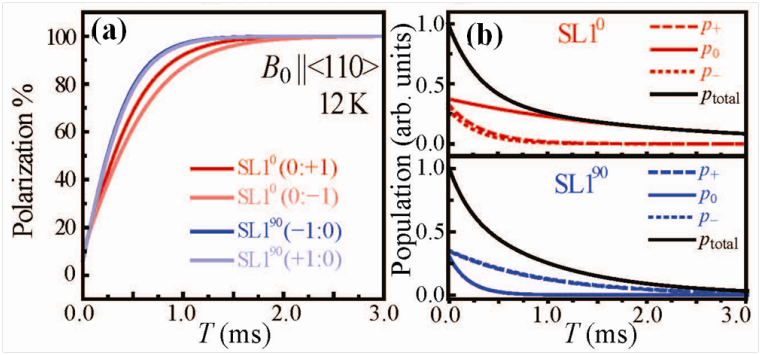

Figure 4.6: Polarization - (a) The polarization build-up and (b) triplet population as a function of waiting time T after the laser pulse.

4.2 Electron spin echo envelop modulation

Figure 4.7(a) shows the electron spin (e-spin) precessing around the applied magnetic field (B_0). However, the nearby nuclear spin feels not just the applied magnetic field but also the local field created by the electron spin, thus tilting the precession axis of the nuclear spin (B_{eff}). The slow precession of the nuclear spin generates time varying oscillating magnetic field ($\Delta B_n(t)$) which modulates the electron spin precession. This modulation will be reflected in the echo decay of the electron spin. Such echo decay profile superimposed with strong modulation is known as electron spin echo envelop modulation (ESEEM).

Lets consider the quantum mechanical approach to explain this more qualitatively. The echo decay profile is superimposed with strong modulations known as ESEEM due to the presence of anisotropic hyperfine interaction of the electron spin with neighboring nuclear spins [5, 6]. The spin Hamiltonian of a single S=1 interacting with a nuclear spin of I is given by

$$\mathcal{H}_{e-n} = \mathcal{H}_e - \mu_n g_n \boldsymbol{B}.\mathbf{I} + AS_ZI_Z + BS_ZI_X, \tag{4.7}$$

where A and B are the secular and pseudo-secular term of the hyperfine coupling. Due to the presence of pseudo secular term, the nuclear spin in the close vicinity of the electron is quantized along an effective magnetic field that is titled from the electron spin quantization axis $Z \parallel B_0$. This leads to the mixing of the nuclear-spin states and application of intense microwave pulse resonates not only the EPR-allowed transitions but also the EPR-forbidden transitions that involve the nuclear-spin flipping. The interference between these transitions generates beats in the electron spin echo decay curve. The fourier transform of such modulated echo will give the weak hyperfine

coupling strength which are unresolved in the EPR spectrum. Figure 4.7(b) shows the SL1 structure with the possibility of nuclear spin at "i/j" or "k/l" site. The nuclear spin at "i/j" are strongly coupled to the electron spin and are well resolved in the EPR spectrum (as shown in Figure 4.2) and will "not contribute" to the modulation of echo profile. However, there is a possibility of nuclear spin present at "k/l" site and such hyperfine coupling has not been resolved till date. In this chapter we use the ESEEM spectroscopy to understand the triplet electron spin environment in more detail.

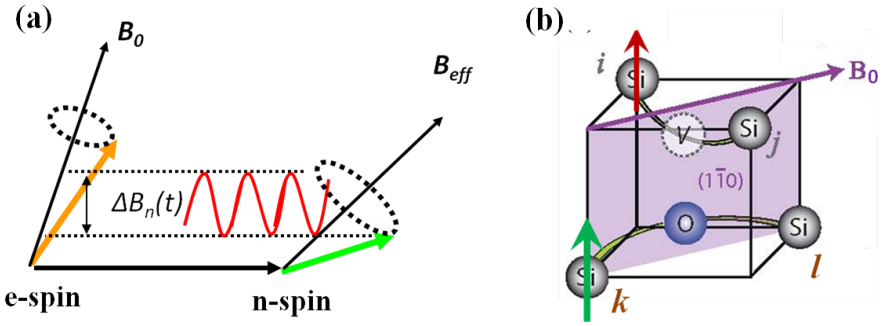

Figure 4.7: Electron spin coupled to a nearby nuclear spin - (a) Schematic showing an electron spin (e-spin) hyperfine coupled to the nuclear spin (n-spin) at its vicinity. The precession axis of the n-spin is tilted and along the effective magnetic field (B_{eff}). The oscillating magnetic field ($\Delta B_n(t)$, sine-wave) that modulates the electron spin is shown. (b)SL1 structure showing the possibility of nuclear spin present at "i/j" or "k/l" lattice site.

Figure 4.8(a) shows the splitting in the triplet sublevels due to the hyperfine interaction with a I=1/2 nuclear spin. The hyperfine splitting frequency of the m_s state to the first order is given as

$$\nu_{ms} = \sqrt{(\nu_I - m_s A)^2 + (m_s B)^2} \tag{4.8}$$

where ν_I represents the Zeeman frequency of the nuclear species causing modulations with amplitude given by the modulation depth parameter $k_m = (\nu_I B/\nu_\alpha \nu_\beta)^2$,where ν_α and ν_β represents the hyperfine splitting in the two spin manifold involved in the EPR transition. In particular, for S=1, the modulation depth is reduced to k_m=$(B/\nu_{\pm 1})^2$, since either ν_α and ν_β is always equal to ν_I. For the two-pulse ESEEM obtained by Hahn echo sequence (Figure 4.8(b)), the modulation involves the two fundamental frequencies (ν_α, ν_β) and also the sum and difference of these frequencies.

Figure 4.8(d) show the two-pulse ESEEM signal from the SL1[90] center for the m_s=-1 to m_s=0 transition (B_0=334.5 mT). In the frequency domain spectrum obtained by

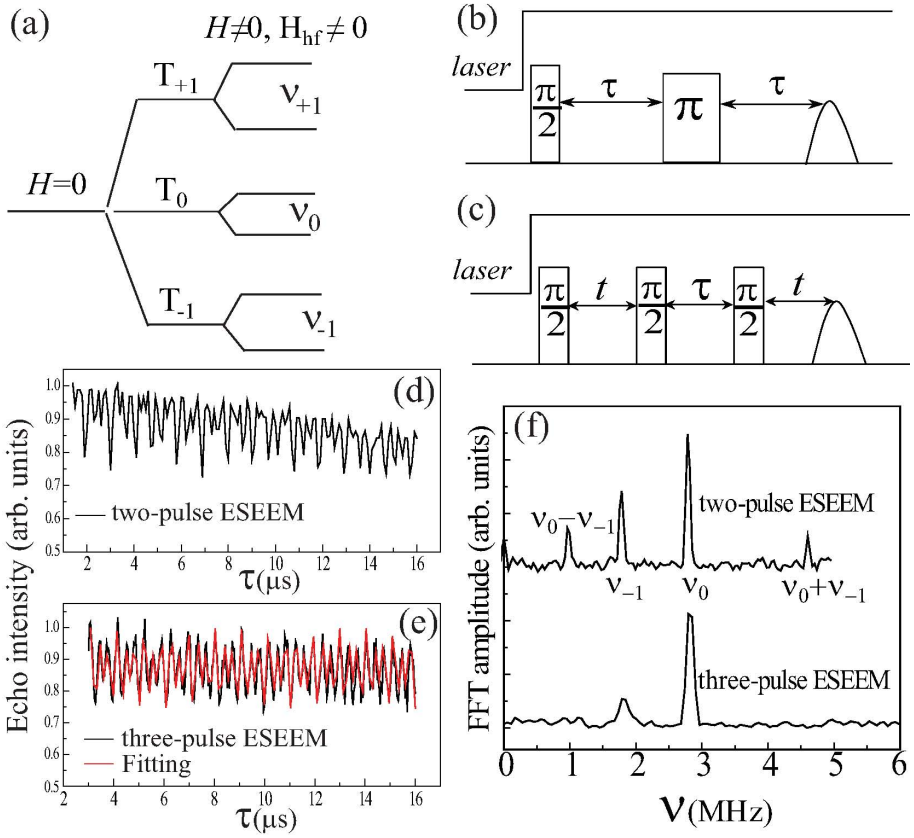

Figure 4.8: Electron echo modulation - (a) Energy levels of the SL1 triplet electron spin interacting with a nuclear spin I=1/2. The pulse sequence employed for observing (b) two-pulse and (c) three-pulse ESEEM . (d) Two-pulse ESEEM and (e) Three-pulse ESEEM signal for the m_s=-1 to m_s=0 transition of the $SL1^{90}$ orientation. The red curve is the fit to the experimental data points using the theoretical expression for three-pulse ESEEM. (e) The frequency domain spectra obtained by the Fourier transform of the ESEEM signal after subtraction of decay part.

Fourier transform of two-pulse ESEEM signal, as shown in Figure 4.8(f), the peaks at 1.8 MHz (ν_{-1}) and 2.8 MHz (ν_0) can be assigned as the fundamental frequencies involved in modulation while 4.6 MHz and 1.0 MHz would be the sum and the difference of the fundamental frequencies, respectively. In order to confirm this we performed three-pulse ESEEM (stimulated spin echo) with the sequence $\pi/2 - t - \pi/2 - \tau - \pi/2 - t - echo$. In three-pulse ESEEM, second $\pi/2$ pulse transfers the electron spin coherence into nuclear spin coherence which during the evolution time τ decays on the order of spin lattice relaxation T_1 of the electron spin and hence the echo can be observed for longer time period as compared to that in two-pulse ESEEM. The third $\pi/2$ pulse transfers

the nuclear spin coherence back to observable electron spin coherence. The added advantage of the 3-pulse ESEEM experiment lies in the fact that modulation contains only the fundamental frequencies which make the frequency domain spectrum much simpler. The three-pulse ESEEM spectrum and its Fourier transform for the above mentioned EPR transition is shown in Figure 4.8 (e) and (f), respectively. This result corroborates our conclusion that 1.8 MHz and 2.8 MHz are the fundamental frequencies in the observed echo modulations. The natural silicon sample contains nearly 4.7% ^{29}Si, the only stable isotope of silicon with a non-zero nuclear spin I=1/2, and its gyromagnetic ratio of 8.46 MHz/T corresponds to the nuclear Zeeman frequency (ν_I) of 2.8 MHz at 334.5 mT. Therefore,we conclude that the observed modulations are due to the hyperfine interaction with a ^{29}Si nuclear spin and the 2.8 MHz and 1.8 MHz peaks (Figure 4.8(f)) corresponds to the splitting in the m_s=0 and m_s=-1 manifolds, respectively. These results illustrate the hyperfine coupling between the SL1 triplet electron spin and ^{29}Si nuclear spin in its vicinity which are too weak to be resolved in the EPR spectrum.

ESEEM has also been reported for phosphorus doped silicon and the observed frequencies were assigned to the hyperfine interaction with the four nearest neighbor ^{29}Si (shell E) [7]. For SL1 center, the nearest neighbor nuclear spins at i or j site (Figure 4.7) has strong enough hyperfine coupling to be resolved in EPR spectrum (Figure 4.2) and cannot contribute to the observed ESEEM. Thus, considering the localized nature of the SL1 triplet electrons, we would conclude that the ESEEM for these triplet centers has a dominant contribution from ^{29}Si present at k or l lattice site (Figure 4.9). This conclusion is further substantiated as we observed splitting in the ESEEM peaks when the magnetic field is rotated in (110) plane. Figure 4.9 shows the frequency domain spectrum of the two-pulse ESEEM signal obtained from the SL1^{90} center for m_s=-1 to m_s=0 transition with the magnetic field (B_0=333.8 mT) tilted by 15° from [1$\bar{1}$0]. Under this condition, the vectors joining the nuclear spins at the k and l sites to the triplet electron spin make different angles with respect to the applied field, giving different anisotropic hyperfine coupling strengths for the two nuclear sites. This result in the observed splitting of 0.12 MHz in the Fourier transformed spectrum. The ν_0 line at 2.8 MHz in Figure 4.9 does not show any splitting because the m_s=0 manifold has no first order hyperfine interaction.

We observed modulation even from the SL1^0 orientation for the m_s=0 to m_s=+1 transition (B_0=353.9 mT), where the echo decay signal modulated with frequency ν_0 = 3.0 MHz and ν_{+1} = 0.6 MHz and their sum (3.6 MHz) and difference (2.4 MHz).

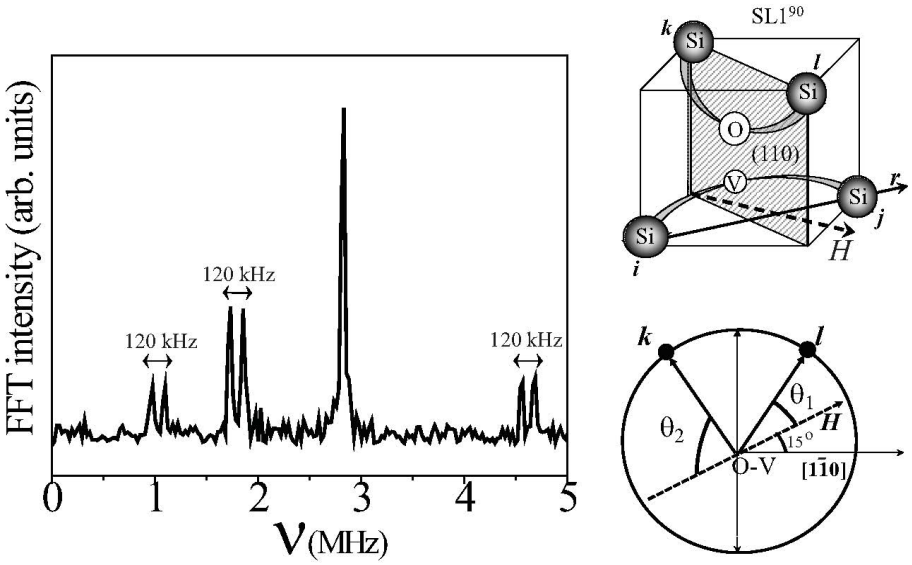

Figure 4.9: Splitting in the frequency domain spectrum of ESEEM - Frequency domain spectrum of two-pulse ESEEM for the $SL1^{90}$ center with the magnetic field B rotated about [110] axis by an angle of 15° from [1-10] direction. The splitting of 0.12 MHz is observed in the line around 1 MHz, 1.8 MHz and 4.6 MHz and attributed to the non-equivalent nuclear spins at k and l sites as the magnetic field is rotated in the (110) plane. The line at 2.8 MHz which corresponds to the energy separation in the m_s=0 manifold (nuclear Zeeman energy) does not split as m_s=0 has no first order hyperfine interaction.

The ESEEM frequency for the different orientation of the SL1 center indicates that the sign of the hyperfine coupling from a nearby nuclear spin depends on the defect orientation, i.e. A<0 for $SL1^0$ and A>0 for $SL1^{90}$. The observation of such weak hyperfine interaction of SL1 center with the neighboring nuclear spin using ESEEM spectroscopy would help in understanding the electron wavefunction of the defect.

From fitting to the three-pulse ESEEM signal for the high-field lines in the EPR spectrum, the modulation depth parameter k_m was found to be 0.40 and 0.18 for $SL1^0$ and $SL1^{90}$ center, respectively. Thus, pseudo secular term $\mid B \mid$ is estimated to be 0.37 MHz and 0.77 MHz for $SL1^0$ and $SL1^{90}$, respectively.

4.3 Conclusion

With the help of electron spin echo experiments using pESR spectroscopy on the excited triplet state of oxygen-vacancy complex, we have characterized the relative populating and decay rates of the triplet sublevels in the presence of magnetic field. The decay process was found to be spin selective and depends significantly on the direction of the applied magnetic field in contrast to the equal populating rate of the sublevels. We showed that this difference in decay rates to the ground singlet state leads to nearly $\sim$100% electron spin polarization within the triplet. The modulations in the echo decay reflect the weak coupling between electron spin of SL1 centers and ^{29}Si nuclear spin present at neighboring sites which are not resolved in the cwEPR spectra. Our experiments suggest that the observed modulation in echo decay is due to the presence of ^{29}Si nuclear spin present at silicon sites bonded by oxygen atom of the SL1 defect.

Bibliography

[1] K. L. Brower, Phys. Rev. B **4**, 1968 (1971). (Cited on page 59.)

[2] L. S. Vlasenko, Yu. V. Martynov, T. Gregorkiewicz, and C. A. J. Ammerlaan, Phys. Rev. B **52**, 1144 (1995). (Cited on page 59.)

[3] L. S. Vlasenko, I. M. Zaritskii, A. A. Konchits, B. D. Shanina, Sov. Phys. Solid State, **26**, 66 (1984). (Cited on page 59.)

[4] A. M. Frens, M. E. Braat, A. B. van Oosten and J. Schmidt, Mat. Sci. Forum, **117**, 195 (1993). (Cited on page 63.)

[5] W. B. Mims, Phys. Rev. B, **5**, 2409 (1972). (Cited on page 64.)

[6] A. Schweiger and G. Jeschke, Principles of Pulse Electron Paramagnetic Resonance (Oxford University Press, Oxford, 2001). (Cited on page 64.)

[7] E. Abe, A. M. Tyryshkin, S. Tojo, J. J. L. Morton, W. M. Witzel, A. Fujimoto, J. W. Ager, E. E. Haller, J. Isoya, S. A. Lyon, M. L. W. Thewalt, and K. M. Itoh, Phys. Rev. B **82**, 121201(R) (2010). (Cited on page 67.)

Chapter 5

Coherent storage of photoexcited triplet states using ^{29}Si nuclear spins in silicon

---

In the previous chapter it was revealed that the lifetime of the m_s=±1 sublevels differ significantly from that of its m_s=0 states of oxygen-vacancy complex. Making use of such a difference in the decay times to the ground singlet state, we can achieve nearly ∼100% electron polarization within the triplets. Here, we demonstrate the transfer of the triplet electron states to the hyperfine coupled, nearest neighbor ^{29}Si nuclear spins, manipulate the ^{29}Si states by resonant pulsed RF fields, and transfer them back to the triplet electrons to be readout by conventional two-pulse electron spin echo. The coherence time of ^{29}Si nuclear spins employed in this operation is shown to be much longer than the lifetime of triplet electrons indicating the great advantage of these nuclear spins in silicon as memory qubits.

5.1 Introduction

Nuclear spins in solids are promising candidates for quantum bits (qubits) as their weak coupling to the environment often leads to very long spin coherence times [1, 2, 3, 4]. However, performing fast manipulation and controlling interaction between nuclear spin qubits is often more challenging than in other, more engineered, quantum systems [5, 6, 7]. The use of an optically driven mediator spin has been suggested as a way to control coupling between donor electron spins in silicon (see Figure 5.1): the donor spins exhibit weak direct coupling, but mutually couple through the optically excited state of the mediator [8]. Such ideas could similarly be applied to couple nuclear spins, and, if the mediator spin is a photo-excited triplet with a spin-zero single ground state, it would have the added advantage that it avoids long-term impact on the nuclear spin coherence [9, 10, 11].

Photoexcited triplets are optically-generated electron spins ($S = 1$) which often exhibit large (positive or negative) spin polarization, thanks to preferential population of each of the triplet sub-levels following intersystem crossing and/or the differing decay rates of these sub-levels to the ground singlet state [12, 13]. Nuclear spins, in contrast, have weak thermal spin polarization at experimentally accessible conditions, due to its small magnetic moment. Highly polarized electron spin triplets can be used to polarize surrounding nuclear spins, through continuous wave microwave illumination (under processes termed dynamic nuclear polarization) [14, 15], or using microwave pulses [16]. Triplet states can also be used to mediate entanglement between mutually-coupled nuclear spins [9], on timescales much faster than their intrinsic dipolar coupling [17].

In this chapter we use the high spin polarization of the triplet system and its strong coupling with the nearest neighbor ^{29}Si nuclear spins to demonstrate coherent state transfer between the electron and nuclear spin degrees of freedom, and examine the nuclear spin coherence in the presence of the triplet.

5.2 Experimental

Cz-grown, single-crystal natural silicon (4.7% ^{29}Si, $I = 1/2$) was exposed to 1 MeV e-beam irradiation (dose $\approx 10^{18}$ cm^{-2}) at room-temperature to form O-V complexes (an interstitial oxygen already present in the silicon traps a mono-vacancy generated due to the e-beam irradiation). Such high doses of e-beam irradiation will generate nearly 10^{16} cm^{-3} SL1 centers under illumination with above band-gap light. Pulsed EPR measurements were carried out at X-band (9.72 GHz) on a Bruker Elexsys580

spectrometer equipped with a helium-flow cryostat. Photoexcitation of the SL1 was achieved using a 1064 nm pulsed Nd:YAG laser (pulse width $\sim$ 7 ns, 1 mJ/pulse) with a 10 Hz repetition rate.

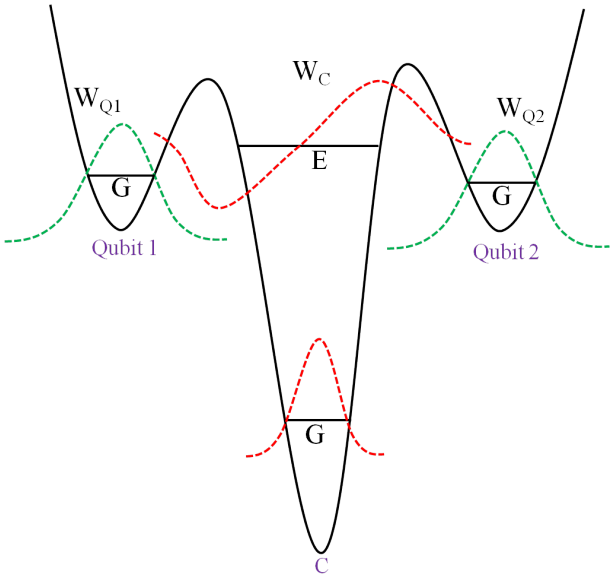

Figure 5.1: Entanglement via excited state - A shematic showing the use of excited state of the atom "C" to entangle remote qubits (Q1, Q2) in the lattice. Qubits Q1 and Q2 in their ground state have wavefunction W_{Q1} and W_{Q2}, respectively. W_C represent the wavefunction of the atom "C" in its excited state.

5.3 Coherent state transfer between photoexcited triplets electron spin and ^{29}Si nuclear spin in silicon

The strong hyperfine coupling between the triplet electrons and nearest neighbor ^{29}Si nuclear spin will split the triplet energy levels, as shown in Figure 4.1. For the following experiments, we focus on four selected levels labeled $|1\rangle, |2\rangle, |3\rangle$ and $|4\rangle$ in Figure 5.2(b) of SL1^{90} corresponding to the electron spin m_s=+1,0 and nuclear spin m_I=±1/2.

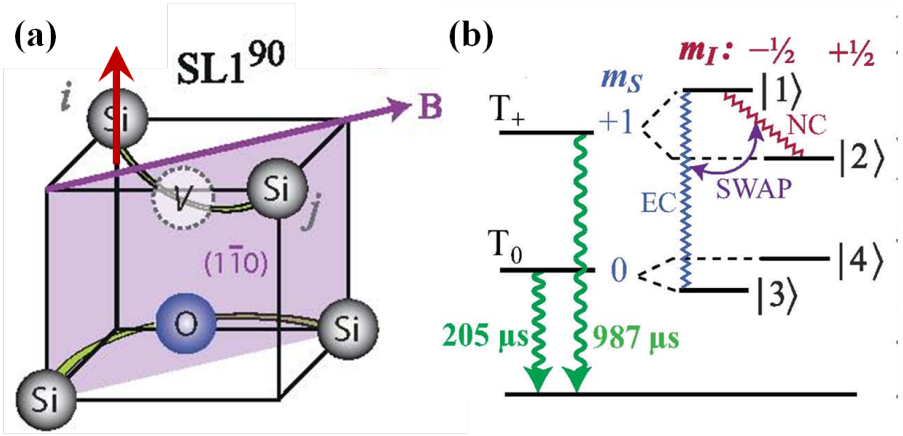

Figure 5.2: Hyperfine coupling between ^{29}Si nuclear spin and SL1 center - (a) SL1^{90} structure showing nearest neighbor ^{29}Si nuclear spin (red arrow) strongly hyperfine coupled to the triplet spin system. (b) Energy level of the triplet spin system due to the coupling with nuclear spin $I = 1/2$. The figure also shows the swapping between the electron and nuclear spin coherence.

The hyperfine coupling strengths between the ^{29}Si nuclear spin and triplet electron spin are studied by the Davies electron-nuclear double resonance (ENDOR) pulse sequence (Figure 5.3(a)). It should be noted that the detection scheme used here is sensitive only to the electron spin, therefore changes brought by the pulse sequences in the nuclear spin states are detected via electron spins. As for the SL1^{90}, m_s=0 is the faster decaying state than the m_s=±1 (see Table 1, Chapter 4), the delay of 700μs after the laser pulse results in the initialization of spin system in the state 1 and 2. A selective microwave π-pulse between $|1\rangle$ and $|3\rangle$ creates a polarization across the nuclear spin transitions, which can be driven using a radiofrequency ($\nu_{\rm rf}$) pulse. The ENDOR signal is obtained by monitoring the electron spin echo on the $|1\rangle$:$|3\rangle$ transition as a function of $\nu_{\rm rf}$. Figure 5.3(a) shows the $|1\rangle$:$|2\rangle$ transition frequency dominated by the strong hyperfine interaction. Thus, with resonant rf pulses we can selectively address ^{29}Si nuclear spins at specific lattice sites i and j. Figure 5.3(b) shows the pulse sequence

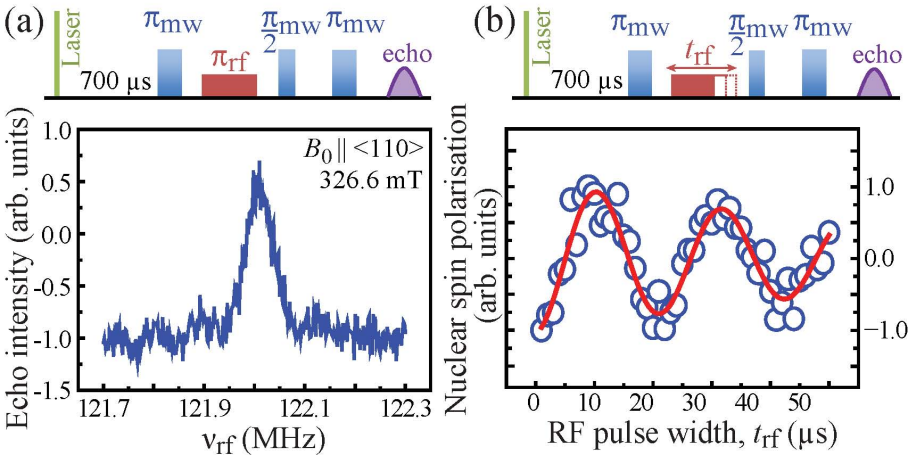

Figure 5.3: ENDOR and nuclear Rabi oscillation - (a)The Davies-ENDOR pulse sequence and the observed ENDOR spectrum. The ENDOR frequency represents the hyperfine strength in the m_s=+1 state of the SL1^{90} center. (b) Rabi oscillation of the ^{29}Si nuclear spins situating at i or j lattice site. Nuclear Rabi oscillation is driven between the states 1 and 2 of Fig. 1(b). The red curve is a fitting function representing exponentially decaying harmonic oscillation.

employed to experimentally demonstrate the manipulation of these ^{29}Si nuclear spins. The echo intensity monitored as a function of resonant RF (122 MHz) pulsewidth that generates Rabi oscillation between state $|1\rangle$ and $|3\rangle$ is shown in Figure 5.3(b). The result indicates the feasibility of using photoexcited triplets to prepare and readout the ^{29}Si nuclear spin state in silicon.

Figure 5.4(a) shows the pulse sequence employed to demonstrate the coherence transfer [4] between the coupled triplet electron spins and nuclear spins in silicon. Figure 5.4(b) represents the energy levels relevant to the coherent transfer experiment. A electron spin coherence between the states $|1\rangle$ and $|3\rangle$ generated by the initial microwave $\pi/2$-pulse is refocused by the next microwave π-pulse. The successive radio frequency (RF) and microwave π-pulse transfers the electron coherence to the nuclear manifold which is refocused by the RF π-pulse. Finally, we transfer the nuclear coherence back to the electron spin and readout is made with the conventional electron spin Hahn echo sequence. The decay of the recovered spin coherence as a function of the storage time in the nuclear spin ($2\tau_n$) is shown in Figure 5.4(c), with an exponential decay of time-constant 0.9(1) ms. The measured decay is dominated by the relaxation of the T_+ sub-level back to the ground singlet state ($1/k_+ = 987$ μs), rather than ^{29}Si nuclear decoherence. The fidelity of the coherent transfer depends upon the ability to recover any

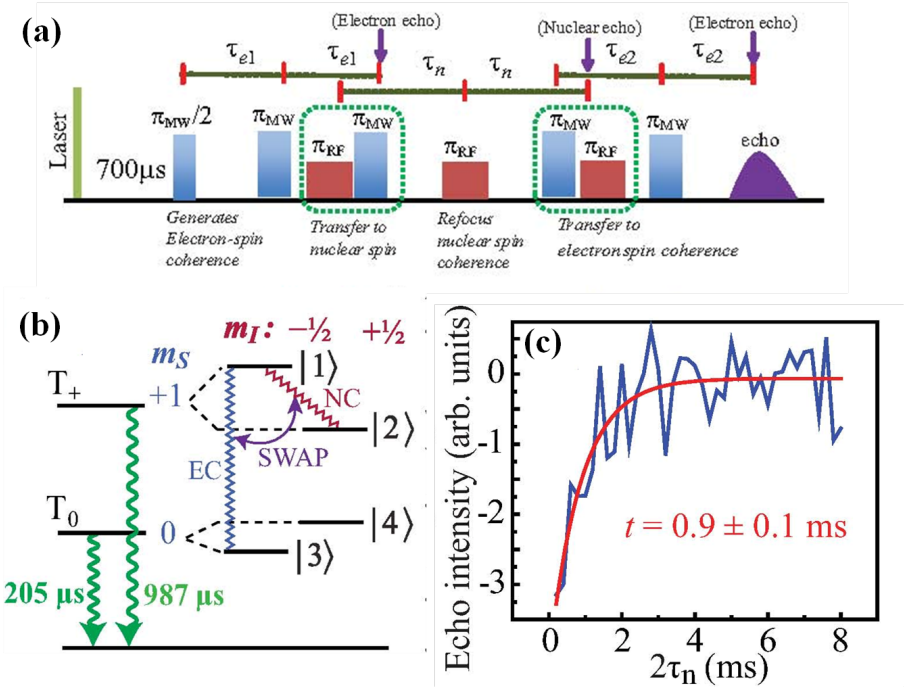

Figure 5.4: Coherent state transfer - (a) The pulse sequence employed for the coherence transfer from the triplet electron spins to ^{29}Si nuclear spin and back to the triplet electron spins. (b) A schematic of the energy levels showing the electron (EC) and nuclear (NC) coherence investigated in this study. (c) Retrieved electron spin echo intensity as a function of the ^{29}Si nuclear storage time, $2\tau_n$. The experimental data (blue curve) with a single-exponential fitting (red curve) yield memory time of 0.87 ms in the T_+ subspace, which is limited by the lifetime 0.96 ms of the T_+ state.

input state of the electron spin after storage in the nuclear spin. Due to sharp ENDOR line (67 kHz) we can excite the full nuclear transitions by using short radio frequency pulses and therefore the stored coherence in the nuclear subspace can be completely transfered to the electron spins. This suggest that the fidelity of the coherent transfer could be on the higher side limited mainly by the fluctuating environment around the spin system. However we still need some more quantitative analysis to give an exact figure for the fidelity of coherent transfer.

In the previous section we showed that the ^{29}Si nuclear coherence was limited by the lifetime of the triplet state. The intrinsic ^{29}Si nuclear coherence is measured using the pulse sequence as shown in Figure 5.5. Here we shift the RF pulses within a fixed experimental window of 1 ms in order to remove the effect of the triplet relaxation and directly measure the ^{29}Si coherence time [18]. The sequence is based on Davies

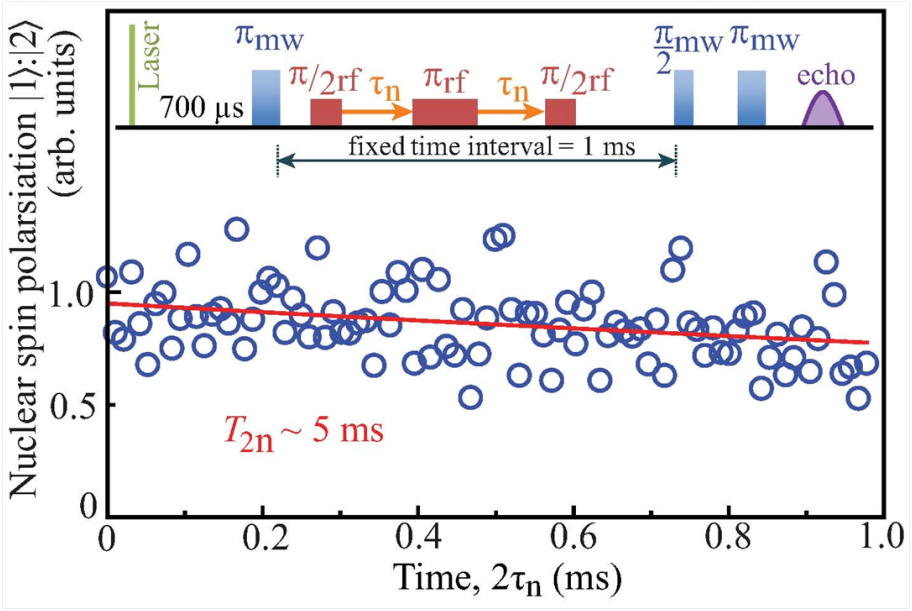

Figure 5.5: Intrinsic nuclear coherence time - The inset shows the pulse sequence employed to estimate the "intrinsic coherence time" of the nuclear spin by fixing the experimental time window to the lifetime (1 ms) of the triplet state. The blue circles are the experimental data obtained by monitoring the echo intensity as a function of the time x. Phase cycling sequences were used to confirm here that the retrieved electron-spin echos were purely due to the transfer of coherence from the nuclear spins.

ENDOR described above, but with the single rf π pulse replaced with a nuclear Hahn echo sequence, whose delay time τ_n is swept. In the absence of nuclear spin decoherence, the applied rf pulses form a net 2π rotation. In contrast, when the nuclear spin is fully decohered, the nuclear spin polarisation across the $|1\rangle$:$|2\rangle$ transition falls to zero.

Fitting the data to an exponential decay gives the nuclear coherence time of 5(1) ms, which should be interpreted as a lower bound. The bulk value for T_{2n} of ^{29}Si in natural silicon has been measured by NMR and found to be 5.6 ms, limited by ^{29}Si dipolar coupling [19]. The hyperfine coupling to the triplet can suppress decoherence from ^{29}Si dipolar coupling as well as introduce additional decoherence mechanisms of its own, though the net result is a measured T_{2n} which is at least as long the bulk value.

5.4 Conclusion

In conclusion, we utilized the coupling between nuclear spin and photoexcited electron spin triplet in silicon to demonstrate the coherent storage and retrieval of triplet electron spin coherence in the ^{29}Si nuclear spin. This motivates further studies in how the nuclear spin state survives the decay to the ground singlet state, as well as the application of NMR pulse sequences to remove the effect of nuclear spin dipolar couplings to achieve coherence times of up to 25 seconds [3]. Furthermore, given the well-developed silicon isotope engineering [20, 21] it will be possible to investigate more than one nuclear spin strongly coupled to the single electron spin in the photoexcited triplet state and explore optical control of the interaction between the nuclear spins.

Bibliography

[1] T. D. Ladd, J. R. Goldman, F. Yamaguchi, Y. Yamamoto, E. Abe, and K. M. Itoh, Phys. Rev. Lett. **89**, 017901 (2002). (Cited on page 72.)

[2] K. M. Itoh, Solid State Commun. **133**, 747 (2005). (Cited on page 72.)

[3] T. D. Ladd, D. Maryenko, Y. Yamamoto, E. Abe, and K. M. Itoh, Phys. Rev. B **71**, 014401 (2005). (Cited on pages 72 and 78.)

[4] J. J. L. Morton, A. M. Tyryshkin, R. M. Brown, S. Shankar, B. W. Lovett, A. Ardavan, T. Schenkel, E. E. Haller, J. W. Ager and S. A. Lyon, Nature **455**, 1085 (2008). (Cited on pages 72 and 75.)

[5] J. R. Petta, A. C. Johnson, J. M. Taylor, E. A. Laird, A. Yacoby, M. D. Lukin, C. M. Marcus, M. P. Hanson, and A. C. Gossard, Science **309**, 2180 (2005). (Cited on page 72.)

[6] K. C. Nowack, M. Shafiei, M. Laforest, G. E. D. K. Prawiroatmodjo, L. R. Schreiber, C. Reichl, W. Wegscheider, and L. M. K. Vandersypen, Science **333**, 1269 (2011). (Cited on page 72.)

[7] T. Obata, M. P. Ladriere, Y. Tokura, Y. Shin, T. Kubo, K. Yoshida, T. Taniyama4, and S. Tarucha, Phys. Rev. B **81**, 085317 (2010). (Cited on page 72.)

[8] A. M. Stoneham, A. J. Fischer and P. T. Greenland, J. Phys. Cond. Mat. **15**, L447 (2003). (Cited on page 72.)

[9] M. Schaffry, V.Filidou, S. D. Karlen, E. M. Gauger, S. C. Benjamin, H. L. Anderson, A. Ardavan, G. A. D. Briggs, K. Maeda, K. B. Henbest, F. Giustino, J. J. L. Morton and B. W. Lovett, Phys. Rev. Lett. **104**, 200501 (2010). (Cited on page 72.)

[10] E. M Gauger, P. P Rohde, A. M. Stoneham and B. W. Lovett, New J. Phys. **10**, 073027 (2008). (Cited on page 72.)

[11] M. Schaffry, B. W. Lovett, and E. M. Gauger, Phys. Rev. A **84**, 032332 (2011). (Cited on page 72.)

[12] J.H.van der Waals, Appl. Magn. Reson. **20**, 545 (2001). (Cited on page 72.)

[13] M. Deimling, H. Brunner, K. P. Dinse, K. H. Hausser, and J. P. Colpa, J. Magn. Reson. **39**, 185 (1980). (Cited on page 72.)

[14] P. Bachert, H. Brunner, K. H. Hausser, and J. P. Colpa, Chem. Phys. **91**, 435 (1984). (Cited on page 72.)

[15] K. Takeda, K. Takegoshi and T. Terao, J. Phys. Soc. Japan **73**, 2319 (2004). (Cited on page 72.)

[16] J. Schmidt, D. J. van den Heuvel, A. Henstra, T.-S. Lin and W. Wenckebach, Pure & App. Chem. **64**, 859 (1992). (Cited on page 72.)

[17] V.Filidou, S. Simmons, S. D. Karlen, H. L. Anderson, F. Giustino, J. J. L. Morton *in preparation* (2011) (Cited on page 72.)

[18] P. Hoefer, A. Grupp and M. Mehring, Phys. Rev. A **33**, 3519 (1986). (Cited on page 76.)

[19] A. E. Dementyev, D. Li, K. MacLean, and S. E. Barrett, Phys. Rev. B **68**, 153302 (2003). (Cited on page 77.)

[20] K. Takyu, K. M. Itoh, K. Oka, N. Saito, and V. I. Ozhogin, Jpn. J. Appl. Phys., Part 2 **38**, L1493 (1999). (Cited on page 78.)

[21] K. M. Itoh, J. Kato, M. Uemura, A. K. Kaliteevskii, O. N. Godisov, G. G. Devyatych, A. D. Bulanov, A. V. Gusev, I. D. Kovalev, P. G. Sennikov, H.-J. Pohl, N. V. Abrosimov, and H. Riemann, Jpn. J. Appl. Phys., Part 1 **42**, 6248 (2003). (Cited on page 78.)

Chapter 6

Summary

6.1 Summary

The present thesis has utilized photoexcited triplet states of oxygen-vacancy centers (SL1 centers) in silicon to probe phosphorus and ^{29}Si spin states using magnetic resonance technique, namely electrically detected magnetic resonance (EDMR) and pulsed electron paramagnetic resonance (pEPR). γ-ray or electron beam irradiation of silicon single crystal lead to the formation of oxygen-vacancy complexes which can be optically excited to the metastable triplet states.

The introduction of such radiation defects in silicon allowed us to detect bulk phosphorus electron and nuclear spins using EDMR spectroscopy. These result is significant for the coherent read out of bulk phosphorus spin states using electrical method. The dipolar interaction between triplet electrons of oxygen-vacancy complexes and phosphorus electron in the bulk lead to the demonstration of electrical detection of cross relaxation (EDCR) where the electron spin of the two paramagnetic centers undergo a flip-flop transition that changes the photoconductivity of the sample. In contrast to EDMR spectroscopy, EDCR does not require any resonance field, thus making it a very simple and sensitive method for the detection of paramagnetic centers in solids.

With the help of electron spin echo experiments using pESR spectroscopy on the excited triplet state of oxygen-vacancy complex, we found the relative populating and decay rates of the triplet sublevels in the presence of magnetic field. It was revealed that the lifetime of the m_s=$\pm$1 sublevels differs significantly from the m_s=0 state, which builds high non-equilibrium spin polarization within the spin system. ESEEM spectroscopy was used to probe the hyperfine interaction between the triplet electron spin of SL1 center and those ^{29}Si nuclear spin which are unresolved in cw-EPR. Frequency-domain analysis unambiguously revealed that the modulation in the echo intensity originates from the interaction between the electron spin and those ^{29}Si nuclear spin which are not resolved in EPR spectrum.

Using such highly polarized electron spin system along with its strong hyperfine

coupling with the nearest neighbor ^{29}Si nuclear spin we experimentally demonstrated ^{29}Si quantum memory in silicon. We successfully transfered the quantum information from the triplet spins to the nuclear spins, manipulated the nuclear spin state and then transfered it back to the electron spins to read out the nuclear state by conventional Hahn echo method. The nuclear coherence shows negligible decay during the lifetime of the triplet spins. These results indicate that the photoexcited triplet can be employed to develop “all silicon quantum computer" using ^{29}Si nuclear spins as qubit. Furthermore, we can also use the optical excitation and de-excitation of triplets to switch “on” and “off” the interaction between the nuclear spin qubits.